

# Dynamic Analysis of the UVMS: Effect of Disturbances, Coupling, and Joint-Flexibility on End-Effector Positioning

Umer Hameed Shah<sup>†‡\*</sup> , Mansour Karkoub<sup>†</sup>,  
Deniz Kerimoglu<sup>†</sup> and Hong-Du Wang<sup>†¶</sup>

<sup>†</sup>Mechanical Engineering Department, Texas A&M University at Qatar, Doha, Qatar  
E-mails: [mansour.karkoub@qatar.tamu.edu](mailto:mansour.karkoub@qatar.tamu.edu), [deniz.kerimoglu@qatar.tamu.edu](mailto:deniz.kerimoglu@qatar.tamu.edu)

<sup>‡</sup>Mechanical Engineering Department, Khalifa University of Science and Technology, Abu Dhabi, UAE

<sup>¶</sup>College of Engineering, Ocean University of China, Qingdao, China  
E-mail: [wanghongdu505@163.com](mailto:wanghongdu505@163.com)

(Accepted January 08, 2021. First published online: February 9, 2021)

## SUMMARY

This paper investigates the dynamics of an underwater vehicle-manipulator system (UVMS) consisting of a two-link flexible-joint manipulator affixed to an autonomous underwater vehicle. The quasi-Lagrange formulation is utilized in deriving a realistic mathematical model of the UVMS considering joints' friction, hysteretic coupling between the joints and links, and the nonlinear hydrodynamic forces acting on the system, such as added mass, viscous damping, buoyancy, drag, and vortex-induced forces. Numerical simulations are performed to demonstrate the effects of hydrodynamic forces and system coupling between the vehicle and the manipulator and the joints and the links on the precise positioning of the end effector.

**KEYWORDS:** Underwater vehicle-manipulator system; Fluid–structure interaction; Underwater robotics; Joint friction and hysteresis; Vortex-induced vibrations; Quasi-Lagrange formulation.

## Nomenclature

Notation	Meaning
$A_p$	Frontal area of an object
$B(x_B, y_B, z_B)$	Center of buoyancy of the vehicle
$c_u, c_v, c_w, c_p, c_q,$ $c_r, c_j, c_{\alpha 1}, c_{\alpha 2}$	Viscous damping coefficients associated with the motion of the vehicle and the manipulator
$C_a$	Added mass coefficient
$C_d$	Drag coefficient
$C_l$	Lift coefficient
$C_v$	Coriolis and centrifugal force matrix in (19)
$d$	Diameter of the cylinder (i.e., vehicle/manipulator's link)
$d_v$	Diameter of the vehicle
$D_v$	Vector of hydrodynamic drag forces on UVMS in (19)
$E_K$	Kinetic energy of the UVMS

\* Corresponding author. E-mail: [umer.umershah@gmail.com](mailto:umer.umershah@gmail.com)

Notation	Meaning
$E_{Ka}$	Kinetic energy of the actuators
$E_{Kl}$	Kinetic energy of the links of the manipulator
$E_{Km}$	Kinetic energy of the manipulator
$E_{Kv}$	Kinetic energy of the vehicle
$E_P$	Potential energy
$f_j$	Dynamic friction torque of the flexible joint
$f_u$	Force input to drive the vehicle along surge direction ( $i_v$ )
$f_v$	Force input to drive the vehicle along sway direction ( $j_v$ )
$f_w$	Force input to drive the vehicle along heave direction ( $k_v$ )
$F_a$	Added mass force
$F_b$	Buoyancy force
$F_C$	Coulomb friction
$F_d$	Drag force
$F_S$	Stribeck friction
$F_v$	Force vector in body-fixed frame
$F_{visc}$	Viscous damping force
$F_{VIV}$	Vortex-induced force
$g$	Gravitational acceleration
$G(x_G, y_G, z_G)$	Center of gravity of the UVMS
$G_v$	Vector of gravity and buoyancy in (19)
$I$	Identity matrix
$J_{1,a}$	Added moment of inertia of link 1
$J_{2,a}$	Added moment of inertia of link 2
$J_{a1}$	Moment of inertia of the rotor of actuator 1
$J_{a2}$	Moment of inertia of the rotor of actuator 2
$J_{ax}$	Added moment of inertia of the vehicle about $i_v$ -axis
$J_{ay}$	Added moment of inertia of the vehicle about $j_v$ -axis
$J_{az}$	Added moment of inertia of the vehicle about $k_v$ -axis
$J_G$	Rotational inertia matrix of the vehicle
$J_{I1}$	Moment of inertia of link 1
$J_{I2}$	Moment of inertia of link 2
$J_{xx}, J_{yy},$ and $J_{zz}$	Moments of inertia of the vehicle about $i_v, j_v,$ and $k_v$
$J_{xy} = J_{yx}, J_{yz} = J_{zy}, J_{xz} = J_{zx}$	Products of the vehicle's inertias about $i_v, j_v,$ and $k_v$
$k_l$	Stiffness of flexible joints (in torsional spring model) of manipulator
$k_m$	Stiffness of the flexible joint connecting manipulator with vehicle
$K$	Stiffness of the flexible joint
$l_1$	Length of link 1
$l_2$	Length of link 2
$l_{c1}$	Position of the CG of link 1 w.r.t. $O_1$
$l_{c2}$	Position of the CG of link 2 w.r.t. $O_2$
$l_v$	Length of the vehicle
$m_1$	Mass of link 1
$m_{1,au}$	Added mass of link 1 along surge direction
$m_2$	Mass of link 2
$m_{2,au}$	Added mass of link 2 along surge direction
$m_{a1}$	Mass of actuator 1
$m_{a2}$	Mass of actuator 2
$m_{mau}$	Added mass of the manipulator along surge direction
$m_{mav}$	Added mass of the manipulator along sway direction
$m_{maw}$	Added mass of the manipulator along heave direction
$m_v$	Mass of the underwater vehicle
$m_{vau}$	Added mass of the vehicle along surge direction
$m_{vav}$	Added mass of the vehicle along sway direction
$m_{vaw}$	Added mass of the vehicle along heave direction
$M_v$	Mass matrix in (19)
$N_r$	Gear transmission ratio of the actuator
$O_1$	Position of joint 1 w.r.t. $O_v$
$O_2$	Position of joint 2 w.r.t. $O_1$
$O-ijk$	Inertial frame
$O_v-i_vj_vk_v$	Body-fixed frame (affixed to the AUV)

Notation	Meaning
$p(t)$	Angular velocity of the AUV about the $i_v$ -axis (roll rate)
$q(t)$	Angular velocity of the AUV about the $j_v$ -axis (pitch rate)
$Q$	Vector of generalized forces
$r(t)$	Angular velocity of the AUV about the $k_v$ -axis (yaw rate)
$r_g$ $r_g = [x_g, y_g, z_g]$	Vector representing CG of the UVMS w.r.t. $O_v-i_vj_vk_v$
$S_t$	Strouhal number
$s_u$	Position of $O_1$ w.r.t. $O_v$ along the $i_v$ -axis
$s_w$	Position of $O_1$ w.r.t. $O_v$ along the $k_v$ -axis
$T$	Coordinate transformation matrix
$u(t)$	Linear velocity of the AUV along the $i$ -axis w.r.t. $O_v-i_vj_vk_v$
$U$	Sea current along the <b><i>i-axis</i></b>
$v(t)$	Linear velocity of the AUV along the $j_v$ -axis (sway) w.r.t. $O_v-i_vj_vk_v$
$v_{c1}$	Velocity of the CG of link 1
$v_{c2}$	Velocity of the CG of link 2
$v_r$	Velocity of the object with respect to the upstream velocity
$v_s$	Shape factor in dynamic friction of the flexible joint
$v_v$	$v_v = [u, v, w]$ , translational quasi velocities
$V$	Sea current along the <b><i>j-axis</i></b>
$V_s$	Volume of submerged body
$w(t)$	Linear velocity of the AUV along the $k_v$ -axis (heave) w.r.t. $O_v-i_vj_vk_v$
$W$	Sea current along the <b><i>k-axis</i></b>
$x(t)$	Position of the AUV along the $i$ -axis (surge) w.r.t. <b><i>O-ijk</i></b>
$y(t)$	Position of the AUV along the $j$ -axis (sway) w.r.t. <b><i>O-ijk</i></b>
$z(t)$	Position of the AUV along the $k$ -axis (heave)w.r.t. <b><i>O-ijk</i></b>
$z_h$	A variable capturing deflection of the hysteretic spring
$\alpha_1$	Angle of link 1 w.r.t. the $i_v$ -axis
$\alpha_2$	Angle of link 2 w.r.t. link 1
$\beta_1$	Actuator angle at joint 1
$\beta_2$	Actuator angle at joint 2
$\varphi(t)$	Roll angle of the AUV w.r.t. <b><i>O-ijk</i></b>
$\theta(t)$	Pitch angle of the AUV w.r.t. <b><i>O-ijk</i></b>
$\psi(t)$	Yaw angle of the AUV w.r.t. <b><i>O-ijk</i></b>
$\omega_1$	$\omega_1 = \alpha'_1$ , angular velocity of link 1
$\omega_2$	$\omega_2 = \alpha'_2$ , angular velocity of link 2
$\omega_3$	$\omega_3 = \beta'_1$ , angular velocity of motor 1
$\omega_4$	$\omega_4 = \beta'_2$ , angular velocity of motor 2
$\omega_v$	Rotational quasi velocities: $\omega_v = [p, q, r]$
$\omega_{vs}$	Vortex-shedding frequency
$\sigma$	The weighting function in hysteresis model
$\rho_w$	Density of water
$\tau_1$	Coupling term between link 1 and joint motor 1
$\tau_2$	Coupling term between link 2 and joint motor 2
$\tau_p$	Torque input to the vehicle to induce roll motion
$\tau_q$	Torque input to the vehicle to induce pitch motion
$\tau_r$	Torque input to the vehicle to induce yaw motion
$\tau_{\beta 1}$	Torque generated by motor 1
$\tau_{\beta 2}$	Torque generated by motor 2
$\Gamma$	The torque transmitted by the hysteretic spring
$\mu$	Stribeck velocity
$\lambda$	Velocity scaling factor
$\eta$	Vector of generalized coordinates
$\xi$	Body-fixed or quasi velocities

## 1. Introduction

An underwater vehicle-manipulator system (UVMS) is an underwater vehicle, such as a remotely operated vehicle (ROV) or an autonomous underwater vehicle (AUV), with a robotic manipulator affixed to it. The UVMS is mostly utilized for performing underwater inspection, maintenance, and

repair tasks requiring high precision, such as plugging, gripping, structural defects detection, fastening, drilling. According to ref. [1], such tasks require a high positioning accuracy of the end effector of the order of a centimeter or less. However, considering the hydrodynamic forces acting on the UVMS and the coupling between the motions of the vehicle and the manipulator, it is a strenuous task to achieve such a high precision of the end effector.<sup>2</sup> To improve the precision of the end effector, control schemes based on vehicle–motion compensation can be applied. However, such schemes rely on the accuracy of the position sensors of the vehicle, which is mostly of the order of a meter and, therefore, cannot effectively meet the precision requirements for positioning the end effector. Therefore, an alternate way of enhancing the precision of the end effector is to pursue model-based control schemes,<sup>3</sup> which requires developing a comprehensive dynamics model of the UVMS. The already existing works on the dynamics of the UVMS overlook some important aspects of coupling that exists within the UVMS components. Such modeling inaccuracies hamper the performance of the model-based control schemes in achieving high precision positioning of the end effector. Therefore, the main aim of this paper is to develop a comprehensive dynamic model of the UVMS to extensively analyze the dynamics of the UVMS in view of the system's coupling and the external nonlinear hydrodynamic forces acting on the system.

Several methods have been used to derive the dynamics equation of the UVMS, such as Newton–Euler method, Kane's method, and the Lagrange method. The UVMS is a highly nonlinear and coupled system that operates in harsh environmental conditions.<sup>4</sup> A proper choice of dynamic models of the UVMS is crucial for the control design due to the extremely complicated and coupled dynamics and uncertain underwater environments. It is desired that the UVMS be modeled with as much detail as possible for simulation purposes. Further, it is also desirable to retain the most significant dynamic effects in the model to simplify the analysis and control design. Moreover, uncertainties in the hydrodynamic parameters and influence of external disturbances, such as ocean currents may be detrimental to the performance of the UVMS. The dynamics of the AUV system without onboard manipulators has already been explored in detail.<sup>5</sup> However, the works investigating the dynamics of the UVMS are limited: In refs. [6]–[10], the dynamic models of the UVMS were derived using the Newton–Euler algorithm, whereas in ref. [11], the quasi-Lagrange method was used. In ref. [12], a dynamic model of an underwater vehicle was developed with a robotic manipulator using Kane's method. The problem of detailed modeling and simulation of the dynamic coupling between an underwater vehicle and manipulator system was studied in ref. [9] considering damping, restoring forces, inertial effects of manipulator mounted on the AUV, and actuator and sensor characteristics.

Considering underwater operation of the UVMS, the dynamics of the manipulator in a fluid environment must be investigated in detail, which involves several hydrodynamic forces, such as the added mass force, viscous damping, buoyancy, drag force, and the vortex-induced forces acting on the UVMS. Although, several existing works have dealt with the effect of drag force on the manipulator,<sup>13–14</sup> the effect of vortex-induced vibrations (VIVs) has not been thoroughly investigated. Whenever a fluid flows past an object, an unstable wake region is formed around the object due to the vortices shed from its structure, which causes the object to vibrate (i.e., vortex-induced vibrations (VIVs)) in the perpendicular direction of the flow.<sup>15–16</sup> Also, due to the fact that the vortex-shedding phenomenon occurs at varying frequencies, VIV is a highly unpredictable and nonlinear phenomenon.<sup>17</sup> The mathematical model, developed in this paper, considers vortex-induced forces acting on the underwater vehicle and investigates the effects of the VIVs transmitted from the vehicle to the manipulator.

The other most important aspect of this study is the integration of the flexibility of joints in the dynamics of the UVMS, which requires the inclusion of the coupling between the vehicle and the manipulator and between the links of the manipulator themselves. Most existing works on the dynamics of the UVMS have considered the joints to be rigid; however, this is not a realistic approach for correctly investigating the responses of a highly coupled system like the UVMS. The control model must incorporate flexibility of the joints connecting the manipulator with the vehicle and the links of the manipulator (i.e., at the motor–link interface) of the robotic manipulator for precise position control of the end effector. Although several works have been reported on the dynamics of flexible-joint manipulators,<sup>18–24</sup> however, as per the best of our knowledge, the effects of the flexibility of the manipulator's joints have not yet been incorporated in the dynamics of the UVMS. Spong<sup>18</sup> modeled the coupling between the link and the actuator as a torsional spring. Such model is quite effective in simulating the actual responses of the flexible joint. However, certain details like damping and

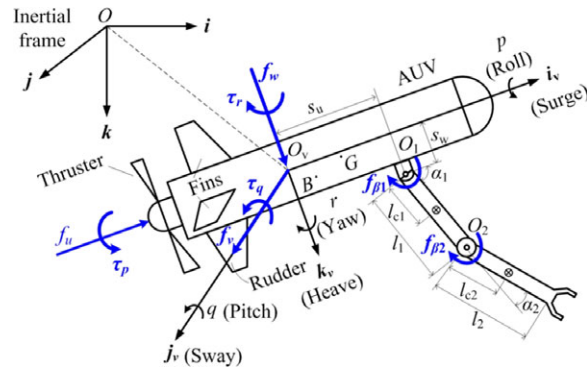


Fig. 1. Schematic of the UVMS.

friction within the flexible joint had been overlooked in the said model. Recently, Ruderman<sup>25</sup> has opted for a more detailed model of the flexible joint, representing it as a hysteretic spring. The said model uses a hysteresis spring to model the energy variation during the operation of a flexible joint. Furthermore, the joint’s friction, which is transmitted from the rotor of the motor to the link, has also been included in the said model. In this work, the joint between the manipulator and the vehicle is modeled using the torsional spring model whereas the manipulator joints are modeled flexible as hysteretic springs with dynamic friction.

In this paper, first, the quasi-Lagrange formulation is utilized in deriving the equations of motion of the UVMS, see Section 2. Based on the developed model, an extensive dynamic analysis of the UVMS is presented in Section 3, which discusses (i) the effect of the flexibility of the joints on the precise positioning of the end effector, (ii) the effect of ocean currents on the dynamics of the UVMS, (iii) the effect of the motions of the vehicle on the dynamics of the end effector considering both rigid and flexible joints between the vehicle and the manipulator, and finally (iv) the effect of the movements of the manipulator on the dynamics of the vehicle. In the end, conclusions are drawn in Section 4, which indicate that the VIVs, the coupling between the subsystems of the UVMS, and the flexibility of joints have a significant impact on precise positioning of the end effector.

**2. Problem Formulation**

Figure 1 depicts the 3D schematic of the UVMS, which consists of an underwater vehicle and a manipulator attached to the vehicle.  $O-ijk$  is the inertial frame whereas  $O_v-i_jv-k_v$  is the moving coordinate system that is affixed to the vehicle and is also called the body-fixed reference frame. For low speed marine vehicles like ROVs and AUVs, the position and orientation of the vehicle are represented relative to the inertial frame,  $O-ijk$ , while the linear and angular velocities are specified with respect to the body-fixed frame,  $O_v-i_jv-k_v$ . In a UVMS, the  $O_v-i_jv-k_v$  frame may not coincide with the center of gravity (CG) and the center of buoyancy of the vehicle, depicted as points  $G$  and  $B$  in Fig. 1, respectively.

**2.1. Kinematics of the UVMS**

The considered underwater vehicle has six degrees-of-freedom (DOF), which include three translational and three rotational motions in the 3D space, and a two-link flexible-joint robotic manipulator. For a manipulator with rigid joints, the DOF equals the number of joint variables, which are the angular displacements of the rotating links. However, in this paper, we are considering elastic- or flexible-joint configuration of the manipulator. In which case, the dynamics of the joint actuators also need to be considered and, consequently, the DOF also include the angular displacements of the shafts of the respective motors. Therefore, for a manipulator having two rigid links and two flexible joints, the  $DOF = 4$ . Consequently, the UVMS with flexible joints has 10 DOF and the vector of the generalized coordinates is given by

$$\eta = [x, y, z, \phi, \theta, \psi, \alpha_1, \alpha_2, \beta_1, \beta_2]^T, \tag{1}$$

where  $x, y,$  and  $z$  are the linear displacements along the  $i, j,$  and  $k$  axes and  $\phi, \theta,$  and  $\psi$  are the angular displacements of the vehicle about the  $i, j,$  and  $k$  axes, respectively, with respect to the inertial frame,

whereas  $\alpha_1$  and  $\alpha_2$  are the angular displacements of link 1 and link 2 and  $\beta_1$  and  $\beta_2$  are the angular displacements of the actuators of joint 1 and joint 2, respectively. Now, from Fig. 1, the kinematic equations of the UVMS can be written as follows.

$$\eta' = T\xi, \tag{2}$$

where

$$\xi = [u, v, w, p, q, r, \omega_1, \omega_2, \omega_3, \omega_4]^T \tag{3}$$

is the velocity vector given with respect to the body-fixed frame (i.e., quasi coordinates) such that  $u, v,$  and  $w$  represent the linear velocities of the underwater vehicle along the  $i_v$  (surge),  $j_v$  (sway), and  $k_v$  (heave) directions and  $p, q, r$  denote the angular velocities of the vehicle about the  $i_v, j_v,$  and  $k_v$  axes, that is, the rates of change of roll, pitch, and yaw motions;  $\omega_1 = \alpha'_1$  and  $\omega_2 = \alpha'_2$  signify the angular velocities of the two links;  $\omega_3 = \beta'_1$  and  $\omega_4 = \beta'_2$  are the angular velocities of the two joint motors, respectively, and

$$T(\eta) = \begin{bmatrix} T_{v_{6 \times 6}} & O_{6 \times 4} \\ O_{4 \times 6} & T_{m_{4 \times 4}} \end{bmatrix} \tag{4}$$

is the non-singular coordinate transformation matrix such that  $TT^T = I_{10 \times 10}$ , where  $I$  is the  $10 \times 10$  identity matrix. In (4),  $T_v = \begin{bmatrix} J_1 & O \\ O & J_2 \end{bmatrix}$  and  $T_m = I_{4 \times 4}$ , where  $J_1$  and  $J_2$  matrices are the linear and angular velocity transformation (i.e., Jacobian) matrices between the inertial and the body-fixed frames, given as follows<sup>11</sup>:

$$J_1 = \begin{bmatrix} \cos\theta \cos\psi & \sin\phi \sin\theta \cos\psi - \sin\psi \cos\phi & \sin\phi \sin\psi + \sin\theta \cos\phi \cos\psi \\ \sin\psi \cos\theta & \cos\phi \cos\psi + \sin\phi \sin\theta \sin\psi & \sin\theta \sin\psi \cos\phi - \sin\phi \cos\psi \\ -\sin\theta & \sin\phi \cos\theta & \cos\phi \cos\theta \end{bmatrix}, \tag{5}$$

$$J_2 = \begin{bmatrix} 1 & \sin\phi \tan\theta & \cos\phi \tan\theta \\ 0 & \cos\phi & -\sin\phi \\ 0 & \sin\phi \sec\theta & \cos\phi \sec\theta \end{bmatrix}. \tag{6}$$

Note: In this paper, the derivatives with respect to time are denoted as  $\frac{d(*)}{dt} = (*)'$ .

2.2. Dynamics of the UVMS considering flexible-joint manipulator

The UVMS is a highly coupled nonlinear system. As discussed earlier in the Introduction section, several methods such as the Newton–Euler method, the Kane’s method, and the Lagrange method can be used to derive the equations of motion of the UVMS. However, according to Sarkar and Podder,<sup>11</sup> since the Lagrangian approach is an energy-based method, it is easier to incorporate the dynamics of new subsystems like additional links or even manipulators in the original model. Further, for the control of the UVMS, it is convenient to deal with the feedback of the deflections/velocities of the manipulator expressed in the body-fixed frame, which requires obtaining the Lagrangian in terms of the body-fixed coordinates rather than the inertial coordinates. In ref. [26], the following form of the quasi-Lagrange formulation, which is the Lagrangian expressed in terms of the body-fixed velocities, was used in obtaining the equations of motion of the UVMS considering rigid joints.

$$\frac{d}{dt} \left( \frac{\partial E_K}{\partial \xi} \right) + T^T \gamma \frac{\partial E_K}{\partial \xi} - T^T \frac{\partial E_K}{\partial \eta} = F, \tag{7}$$

where

$$\gamma = \left[ \xi^T T^T \frac{\partial \Gamma}{\partial \eta} \right] - \left[ \xi^T T^T \left[ \frac{\partial \Gamma}{\partial \eta} \right] \right], \tag{8}$$

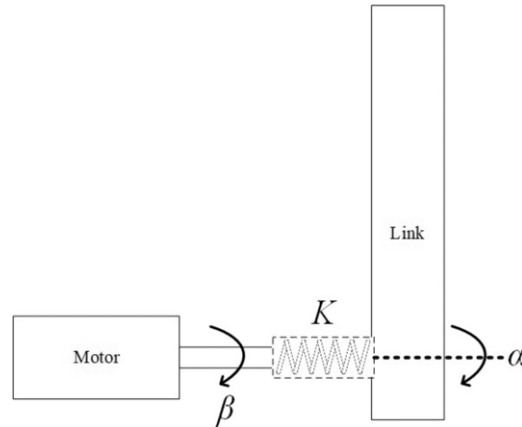


Fig. 2. Schematic of a flexible joint represented as a torsional spring.

$E_K = E_K(\eta, \xi)$  denotes the kinetic energy of the UVMS where  $\eta = [x, y, z, \phi, \theta, \psi, \alpha_1, \alpha_2]^T$  represents the vector of the positions of the vehicle along the *i*-, *j*-, and *k*-axis, the roll, pitch, and yaw angles, and the angles of link 1 and link 2, respectively. The vector  $\xi = [u, v, w, p, q, r, \omega_1, \omega_2]^T$  represents the time derivative of  $\eta$ . The force vector  $F = T^T Q$ , where  $Q$  denotes the vector of the generalized forces acting on the UVMS, includes the control inputs to drive both the vehicle and the manipulator as well as the hydrodynamic forces acting on the system.

In this paper, a dynamic model of the UVMS is developed, which not only includes the manipulator joint flexibility, but also the dynamics of the actuators driving the links. Therefore, the said system has 10 DOF represented by the coordinates vector  $\eta$  defined in (1). For such a flexible-joint configuration, the coupling between the links and their drive motors must be considered as well. Spong<sup>18</sup> modeled a flexible joint as a torsional spring, see Fig. 2, which can be represented by the following phenomena/variables: (i) gear reduction represented by the gear ratio  $N_r$ ; and (ii) the elasticity of the joint represented by  $k_l(\alpha_n - \beta_n)$ , where  $k_l$  denotes the stiffness and the subscript represents the joints' number (i.e.,  $n = 1, 2$ ). This coupling between the links and their drive motors can be represented by the following potential energy term:

$$E_P = \left(\frac{1}{2}\right) \left( k_l(N_r^{-1}\beta_1 - \alpha_1)^2 + K_l(N_r^{-1}\beta_2 - \alpha_2)^2 \right). \tag{9}$$

Furthermore, for the flexible-joint configuration, the total kinetic energy ( $E_K$ ) of the UVMS is the sum of the kinetic energies of the vehicle ( $E_{Kv}$ ), the links of the manipulator ( $E_{Kl}$ ), and the actuators ( $E_{Ka}$ ):

$$E_K = E_{Kv} + E_{Kl} + E_{Ka}. \tag{10}$$

First, the kinetic energy of the underwater vehicle is given as follows:

$$E_{Kv} = \left(\frac{1}{2}\right) (m_v + m_1 + m_2)v_v^T v_v + m_v v_v \cdot (\omega_v \times r_g) + \left(\frac{1}{2}\right) \omega_v^T J_G \omega_v, \tag{11}$$

where  $m_v$  denotes the mass of the vehicle,  $m_1$  is the mass of link 1,  $m_2$  is the mass of link 2,  $v_v = [u, v, w]$ ,  $\omega_v = [p, q, r]$ ,  $r_g = [x_g, y_g, z_g]$  is the position vector representing the CG of the UVMS with respect to the body-fixed frame, and

$$J_G = \begin{bmatrix} J_{xx} & -J_{xy} & -J_{xz} \\ -J_{yx} & J_{yy} & -J_{yz} \\ -J_{zx} & -J_{zy} & J_{zz} \end{bmatrix}, \tag{12}$$

where  $J_{xx}$ ,  $J_{yy}$ , and  $J_{zz}$  denote the moments of inertia of the vehicle about the surge, sway, and heave axes, respectively, and  $J_{xy} = J_{yx}$ ,  $J_{yz} = J_{zy}$ ,  $J_{xz} = J_{zx}$ , are the products of the vehicle's inertias about the respective body-fixed axes.

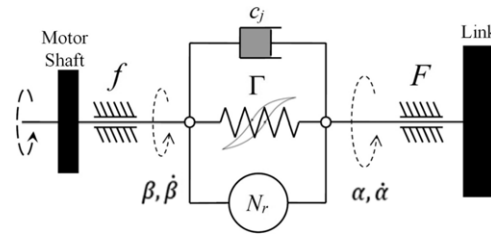


Fig. 3. Schematic of a flexible joint represented as a hysteretic spring.<sup>19</sup>

Now, the kinetic energy of the rigid links of the manipulator is given as follows:

$$E_{KI} = (1/2) ((m_1 v_{c1}^2 + J_{I1} \omega_1^2) + (m_2 v_{c2}^2 + J_{I2} \omega_2^2)), \tag{13}$$

where  $v_{c1}$  and  $v_{c2}$  are the linear velocities of the CGs,  $m_1$  and  $m_2$  are masses,  $J_{I1}$  and  $J_{I2}$  are the moments of inertias, and  $\omega_1$  and  $\omega_2$  are the angular velocities of the two rigid links of the manipulator, respectively. Finally, the kinetic energy of the actuators of the two joints is given as follows:

$$E_{Ka} = (1/2) (m_{a1} v_v^T v_v + m_{a2} v_1^2 + J_{a1} \omega_3^2 + J_{a2} (\omega_1^2 + \omega_4^2)), \tag{14}$$

where  $m_{a1}$  is the mass of the actuator driving link 1,  $m_{a2}$  is the mass of the actuator driving link 2,  $v_1$  is the velocity of the end point of link 1,  $J_{a1}$  and  $J_{a2}$  are the moments of inertias, and  $\omega_3$  and  $\omega_4$  are the angular velocities of the two rotors of the motors driving the links, respectively.

If the flexibility of the joints is considered in the dynamic model, the potential energy terms derived in Eq. (9) must be included in Eq. (7). Therefore, in the presence of the potential energy term due to the consideration of flexible-joint configuration, the quasi-Lagrange equation takes on the following form:<sup>27</sup>

$$\frac{d}{dt} \left( \frac{\partial E_K}{\partial \dot{\xi}} \right) + T^T \gamma \frac{\partial E_K}{\partial \xi} - T^T \frac{\partial E_K}{\partial \eta} + T^T \frac{\partial E_P}{\partial \eta} = F, \tag{15}$$

where  $\eta$  and  $\xi$  are defined in (1) and (3), respectively,  $T$  is shown in (4),  $\gamma$  in (8),  $E_P$  in (9),  $E_K$  in (10)–(14), and the force vector  $F$  comprises the forces and torques to drive the vehicle and the manipulator together with the hydrodynamic forces acting on the UVMS, given in the body-fixed frame as

$$F = [(f_u + F_{h,u}) \ (f_v + F_{h,v}) \ (f_w + F_{h,w}) \ \tau_p \ \tau_q \ \tau_r \ \tau_1 \ \tau_2 \ (\tau_{\beta 1} - \tau_1) \ (\tau_{\beta 2} - \tau_2)]^T, \tag{16}$$

where  $f_u, f_v$ , and  $f_w$  are the thrust forces to move the vehicle along the surge, sway, and heave directions;  $\tau_p, \tau_q$ , and  $\tau_r$  are the torques to induce roll, pitch, and yaw motions in the vehicle;  $F_{h,u}, F_{h,v}, F_{h,w}$  are the components of the hydrodynamic forces acting on the system along the surge, sway, and heave directions, respectively;  $\tau_{\beta 1}$  and  $\tau_{\beta 2}$  are the torques generated by the two motors to drive the links of the manipulator; and  $\tau_1$  and  $\tau_2$  represent the coupling torques between the links and the respective drive motors imparted by the flexibility of the joint. It is to be noted that the forces ( $f_u, f_v$ , and  $f_w$ ) used for translating, and the torques ( $\tau_p, \tau_q$ , and  $\tau_r$ ) used for rotating the vehicle, are generated by a collective action of the vehicle’s thrusters and fins.

In view of (9), when the flexible joints are modeled as a torsional springs,<sup>18</sup> the resulting torques are represented as follows:

$$\tau_n = k_l (N_r^{-1} \beta_n - \alpha_n), \tag{17}$$

where  $n = 1, 2$ . The torsional spring representation of the flexible joint is simplistic and considers only a linear coupling relationship between the angular deflections of the motors and the links. However, according to ref. [28], a flexible link behaves as a hysteretic spring and must also contain viscous damping and dynamic friction terms (i.e., the friction transmitted from motor’s shaft to the link) associated with the joint, see Fig. 3. Now, considering the hysteretic spring configuration of the flexible joint, the coupling terms  $\tau_1$  and  $\tau_2$  are represented as follows:

$$\tau_n = \Gamma(\delta_n) + c_j \delta'_n(t), \quad (n = 1, 2) \tag{18}$$



where  $\delta_n = N_r^{-1} \beta_n - \alpha_n$ ,  $c_j$  is the viscous damping coefficient associated with the hysteresis spring and  $\Gamma$  is the torque transmitted by the hysteretic spring, which can be written using the Bouc-Wen-like hysteretic model as follows:

$$\Gamma(\delta_n) = \sigma K(\delta_n)\delta_n + (1 - \sigma)K(\delta_n) |z_h(t)|, \tag{19}$$

where  $\sigma$  is the weighting function that provides a relationship between a purely elastic (i.e.,  $\sigma = 1$ ) and purely hysteretic (i.e.,  $\sigma = 0$ ) response,  $K(\delta_n)$  is the nonlinear stiffness, and  $z_h$  is a variable which captures the elasto-plastic deflection behavior of the hysteretic spring, given as follows:

$$z_h(t) = \dot{\delta}_n(t) - a \left| \dot{\delta}_n(t) \right| |z_h(t)|^{n-1} z_h(t) - b \dot{\delta}_n(t) |z_h(t)|^n, \tag{20}$$

where  $a$  and  $b$  are the parameters for controlling the amplitude and shape of the hysteresis loop, and  $n \geq 1$  assigns the smoothness of transitions between elastic and hysteretic parts.

Now, the dynamic friction torque  $f_j(\beta')$  of the motor drive can be described using the following friction model given in ref. [25]:

$$f_j(\beta') = \text{sig}(\beta') \left( F_C + F_S e^{[-v_s^{-\mu} |\beta'|^\mu]} \right), \tag{21}$$

$$\text{sig}(\beta') = -1 + \left( 2 / \left( 1 + e^{-\lambda \beta'} \right) \right), \tag{22}$$

where  $\lambda$  is the velocity scaling factor,  $F_C$  and  $F_S$  are the Coulomb and Stribeck friction coefficients such that  $F_C > 0$  and  $F_S > 0$ , the Stribeck velocity  $\mu \neq 0$ , and the shape factor  $v_s > 0$ . Now, considering the flexible joints as hysteretic springs having dynamic friction, the force vector  $F$  in (16) can be rewritten as follows:

$$F = [(f_u + F_{h,u}) \ (f_v + F_{h,v}) \ (f_w + F_{h,w}) \ \tau_p \ \tau_q \ \tau_r \ \tau_1 \ \tau_2 \ (\tau_{\beta 1} - f_1 - \tau_1) \ (\tau_{\beta 2} - f_2 - \tau_2)]^T, \tag{23}$$

where  $\tau_1$  and  $\tau_2$  are given by (18)–(20) and  $f_1$  and  $f_2$  are given by (21)–(22).

**2.2.1. Hydrodynamic forces.** Whenever an object moves in a fluid, the resulting fluid–structure interaction generates hydrodynamic forces that act on the object. Such hydrodynamic forces have a significant impact on the movement of the object in the fluid and consist of the added mass, buoyancy, viscous damping, drag, and vortex-induced forces. The added mass force is the hydrodynamic force exerted on the object by the additional fluid/water displaced by the object itself. Although, it can take on many different shapes, the UVMS is assumed to have a cylindrical shape (torpedo-like). Therefore, from ref. [29], for a translational motion of a cylindrical object, the added mass force is given as follows:

$$F_a = m_a v_r', \tag{24}$$

where  $m_a = (\pi/4)\rho C_a d^2 l$  such that  $\rho = 1,000 \text{ Kg/m}^3$  is the density of water,  $C_a$  is the added mass coefficient, whereas  $d$ ,  $l$ , and  $v_r$  denotes the diameter, length, and relative velocity (with respect to the upstream velocity) of the object, respectively. Motivated by the work of refs. [6, 7], a simplified added mass force is adopted where  $C_a = 1.0$ .

Now, for rotational motion, a resultant moment ( $M_a$ ) due to the displaced fluid acts on the object, which is given as follows:<sup>29</sup>

$$M_a = J_a \alpha'', \tag{25}$$

where  $J_a$  is the added moment of inertia and  $\alpha''$  is the angular acceleration of the object. Here,  $J_a$  is chosen as  $J_a = (1/12)\pi \rho r^2 l^3$ .<sup>6,7</sup>

The buoyancy force is the weight of the water displaced by the volume ( $V_s$ ) of the submerged object and is given as follows:

$$F_b = \rho V_s g, \tag{26}$$

where  $g$  is the gravitational acceleration. The components of the viscous damping forces ( $F_v$ ) opposing the motion of the vehicle can be modeled as  $-c_u u$ ,  $-c_v v$ ,  $-c_w w$ ,  $-c_p p$ ,  $-c_q q$ , and  $-c_r r$ , whereas those for opposing the rotary motion of the links of the manipulator can be modeled as  $-c_{\alpha 1} \alpha'_1$  and  $-c_{\alpha 2} \alpha'_2$  where  $c_u$ ,  $c_v$ ,  $c_w$ ,  $c_p$ ,  $c_q$ ,  $c_r$ ,  $c_{\alpha 1}$ , and  $c_{\alpha 2}$  are the viscous damping coefficients associated with the motion of the vehicle and the links. The drag force has a quadratic form and, formally, it is given as follows:

$$F_d = \left(\frac{1}{2}\right) C_d \rho A_p |v_r| v_r, \tag{27}$$

where  $C_d$  is the coefficient of drag and  $A_p$  is the frontal area of the object. The vortex-induced force acts on the object in the perpendicular direction to the motion (or the impacting sea current).<sup>30</sup> It is caused by the formation of a turbulent wake region around the object, which is a consequence of the shedding of vortices from the structure of the object upon its interaction with the surrounding fluid. The nonlinear vortex-induced force is given by ref. [31]

$$F_{VIV} = \left(\frac{\pi}{4}\right) C_l \rho d v_r^2 \cos(\omega_{vs} t + \vartheta), \tag{28}$$

where  $C_l$  is the lift coefficient,  $\vartheta$  is the phase angle, and  $\omega_{vs}$  is the vortex-shedding frequency given as

$$\omega_{vs} = 2\pi S_t v_r / d, \tag{29}$$

where  $S_t$  is the Strouhal number.

2.2.2. *Equations of motion.* Substituting (9), (10)–(14) into (15), leads to the equations of motion of the UVMS with flexible joints in the following matrix form:

$$M_v \xi' + C_v \xi + D_v \xi + G_v = F_v, \tag{30}$$

where  $M_v$  is the mass matrix that includes the masses of the rigid bodies (i.e., the vehicle, the links of the manipulator, and the actuators of the manipulator) as well as the added masses of the vehicle and the links,  $C_v$  is the Coriolis and Centrifugal force matrix,  $D_v$  is the vector of hydrodynamic drag and viscous damping forces acting on the UVMS,  $G_v$  is the vector of the gravity and buoyancy forces, and  $F_v$  is the vector of external forces acting on the UVMS. It is to be noted that the subscript  $v$  in (30) refers to the matrices obtained with respect to the quasi coordinates (i.e., in the body-fixed frame). The details of matrices  $M_v$ ,  $C_v$ ,  $D_v$ , and the vectors  $G_v$  and  $F_v$ , in (30), are provided online (as Appendix A) at Cambridge Core in supplementary material to this article. Readers may refer to the supplementary material associated with this article, available at Cambridge Core ([www.cambridge.org/core/journals/econometric-theory](http://www.cambridge.org/core/journals/econometric-theory)).

To obtain the responses of the UVMS with respect to the inertial frame, (30) can be written in the following form:<sup>32,33</sup>

$$M \eta'' + C \eta' + D \eta' + G = Q, \tag{31}$$

where  $M = T^{-T} M_v T^{-1}$ ,  $C = T^{-T} [C_v - M_v T^{-1} T'] T^{-1}$ ,  $D = T^{-T} D_v T^{-1}$ ,  $G = T^{-T} G_v$ , and  $Q = T^{-T} F_v$ .

### 3. Dynamic Analysis of the UVMS

The UVMS is a highly coupled nonlinear system. Whenever the UVMS moves in water or encounters ocean currents, the fluid–structure interaction induces VIVs in the structure of the vehicle. The VIVs are then transmitted to the manipulator affixed to the vehicle that, consequently, results in positional inaccuracies and possible wear/damage in the structure of the manipulator. Further, the manipulator, due to its inertia, also affects the dynamics of the vehicle. Other than the vehicle–manipulator coupling, the links of the manipulator are also coupled to the actuators via flexible joints. Such coupling, although overlooked in the existing UVMS dynamic models, has a significant impact on the positioning of the end effector especially during maneuvers requiring high positional precision, for example, welding, screw fastening, tool gripping, etc. Therefore, to investigate the influence of (i) coupling between the vehicle and the manipulator, (ii) the flexibility of the rotational joints of the manipulator,

Table I. Simulation parameters.

Parameters	Values
Mass of the vehicle ( $m_v$ )	53.97 Kg
Length of the vehicle ( $l_v$ )	1.1 m
Diameter of the vehicle ( $d_v$ )	0.25 m
Vehicle's moment of inertia $i_v$ -axis ( $I_{xx}$ )	0.34 Kg-m <sup>2</sup>
Vehicle's moment of inertia $j_v$ -axis ( $I_{yy}$ )	3.71 Kg-m <sup>2</sup>
Vehicle's moment of inertia $k_v$ -axis ( $I_{zz}$ )	3.71 Kg-m <sup>2</sup>
Position of the CG ( $x_g, y_g, z_g$ )	(0, 0, 0) m
Position of the CB ( $x_b, y_b, z_b$ )	(0, 0, 0.015) m
Mass of link 1 and link 2 ( $m_1, m_2$ )	1.5708 Kg
Length of link 1 and link 2 ( $l_1, l_2$ )	0.2 m
Diameter of link 1 and link 2 ( $d_{m1}, d_{m2}$ )	0.025 m
Length of the centroids of links ( $l_{c1} = l_{c2}$ )	0.1 m
Viscous damping coefficients for translation ( $c_x = c_y = c_z$ )	0.01 N-s/m
Viscous damping coefficients for rotation ( $c_\phi = c_\theta = c_\psi = c_{\alpha 1} = c_{\alpha 2} = c_{\beta 1} = c_{\beta 2}$ )	0.02 N-m-s/rad
Moment of inertia of the links ( $I_1$ and $I_2$ )	0.01 Kg-m <sup>2</sup>
Coefficient of drag ( $C_d$ ), <sup>9</sup>	1.25
Lift coefficient ( $C_l$ ), <sup>9</sup>	1.15
Strouhal number ( $S_r$ )	2.0
Coulomb friction coefficient ( $F_C$ )	0.01
Stribeck friction coefficient ( $F_S$ )	0.01
Stribeck velocity ( $\mu$ )	0.1 m/s
Shape factor ( $v_s$ )	0.1
Velocity scaling factor ( $\lambda$ )	0.5

and (iii) the vortex-induced forces on the precision positioning of the end effector, a comprehensive dynamic analysis of the UVMS is presented in this section.

In this section, underwater responses of the end effector resulting from both translational and rotational movements of the vehicle and the manipulator are simulated using MATLAB<sup>TM</sup>. The numerical simulations are generated using the UVMS's equations of motion, (30), and the parameters are listed in Table I. The initial configuration of the UVMS is such that the surge, the sway, and the heave axes of the vehicle are aligned with the  $i$ ,  $j$ , and  $k$  axes of the inertial frame and that both the links of the manipulator are aligned with the heave axis of the vehicle. Three forces are applied to translate, that is, along the  $i_v$ -axis ( $f_u$ ), the  $j_v$ -axis ( $f_v$ ), and the  $k_v$ -axis ( $f_w$ ), and three torques are applied to rotate, that is, about the  $i_v$ -axis ( $\tau_p$ ), the  $j_v$ -axis ( $\tau_q$ ), and the  $k_v$ -axis ( $\tau_r$ ), the vehicle in the 3D space, whereas the  $\tau_{\beta 1}$  and  $\tau_{\beta 2}$  are the torques of the two motors applied at the joints of the manipulator to drive the two links. Furthermore, constant velocity sea currents are also considered to act on the vehicle along the  $i$ -axis ( $U$ ), the  $j$ -axis ( $V$ ), and the  $k$ -axis ( $W$ ), respectively.

First, the effect of the elasticity of joints on the positioning of the end effector is investigated. Three different cases are analyzed while assuming the vehicle to be at rest: (a) when the joints are considered as rigid, (b) when the joints are considered as torsional springs, and (c) when the joints are considered as hysteretic springs. Figure 4(a) compares the dynamic responses of the manipulator for rigid and flexible joint (modeled as torsional spring) configurations when the applied motor torques are  $\tau_{\beta 1} = \tau_{\beta 2} = 0.1$  N-m. The responses represented by the dashed lines refer to the rigid-joint configuration whereas the dash-dot and solid lines correspond to the flexible joint configuration with joint stiffness values of 0.02 and 0.6 N/m, respectively. It is evident that for a higher stiffness value ( $k_l = 0.6$  N/m), the responses are close to those of the rigid-joint configuration. However, for a lower stiffness value ( $k_l = 0.02$  N/m), there is a large deviation of the response from that of the rigid-joint case. It is to be noted that the responses in Fig. 4(a) are obtained for a gear ratio value of  $N_r = 1$ . To depict the effect of variations in the gear ratio on the dynamics of the manipulator, responses of the end effector for  $\tau_{\beta 1} = \tau_{\beta 2} = 0.1$  N-m are shown, in Fig. 4(b), for three different values of gear ratios (i.e.,  $N_r = 1, 10$ , and  $50$ ) while considering a fixed joint stiffness,  $k_l = 0.6$  N/m. The dashed line corresponds to  $N_r = 1$ , the dotted line to  $N_r = 10$ , and the solid line to  $N_r = 50$ . It can be seen that as the gear ratio increases, the response becomes stiffer, manifested in an increase in the torque transmitted to the links from the motors. Figure 4(a) and (b) represent the dynamic responses of the manipulator

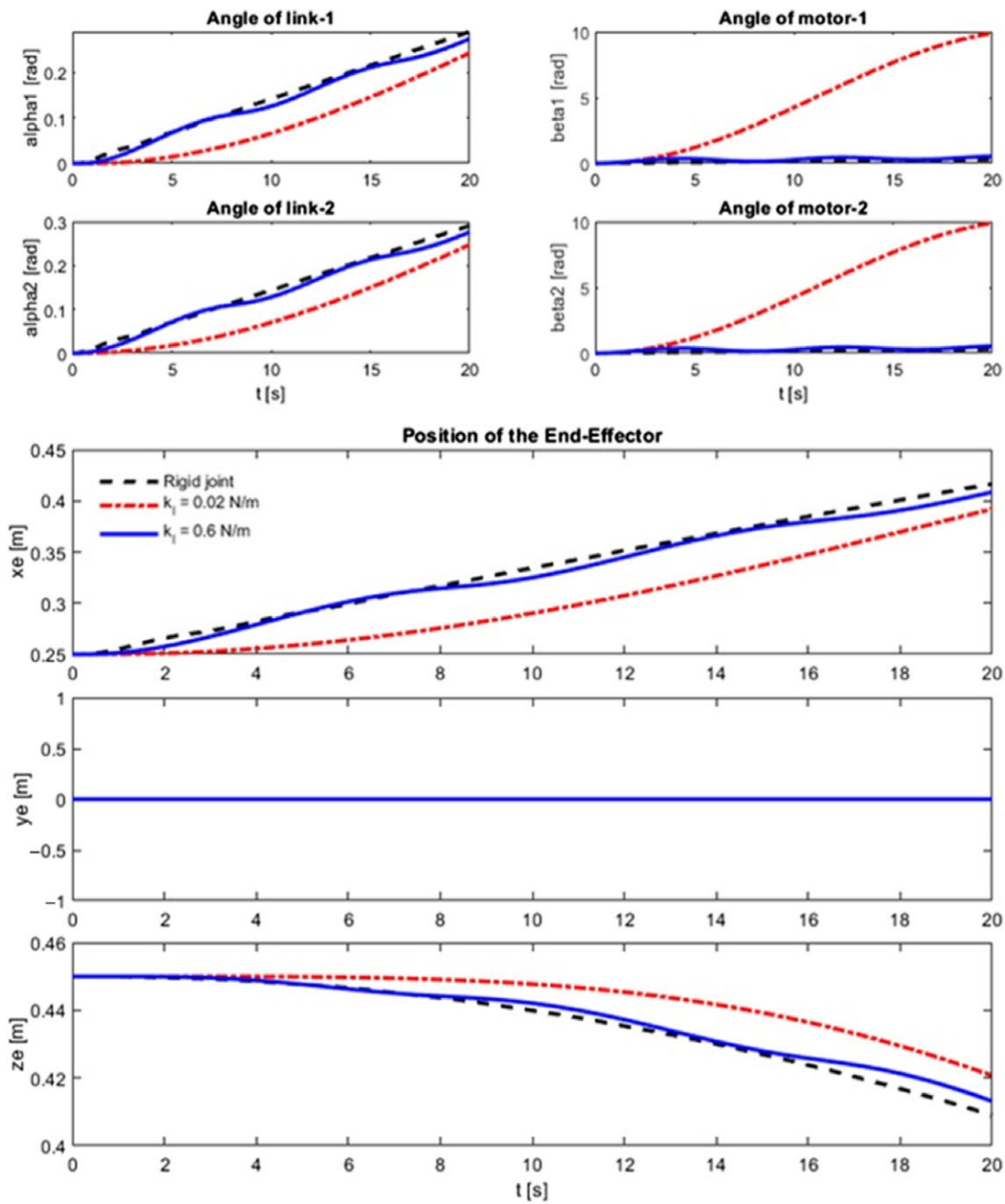


Fig. 4a. Manipulator dynamics with a fixed base – A comparison of rigid-joint configuration with flexible joints modeled as torsional springs with  $N_r = 1$  and varying joint stiffness ( $k_t$ ).

when its joints were modeled as torsion springs. Such a flexible joint model is simplistic and does not cover all the structural aspects of the actual joint. A more realistic approach in modeling the flexible joint is to consider it as a hysteretic spring.<sup>28</sup> The hysteretic spring model considers joint damping ( $c_j$ ), the torque due to the hysteretic spring ( $\Gamma$ ), the gear ratio ( $N_r$ ), and the friction ( $f_j$ ) transferred from the motor’s shaft to the link, see Fig. 3.

Figure 5 compares the responses of the end effector considering rigid- and flexible-joint (modeled as a hysteretic spring) configurations when torques of the two actuators are taken as  $\tau_{\beta 1} = \tau_{\beta 2} = 0.01 \sin(0.5t)$  N-m. Figure 5(a) emphasizes the effect of variation in the joint’s damping on the response of the end effector without considering joint’s friction ( $f_j$ ): The dashed line represents the rigid joint, whereas the dotted, the dash-dot, and the solid lines indicate the responses to the hysteretic spring joint model corresponding to three different values of the joint’s damping (i.e.,  $c_j = 0.01, 0.1,$

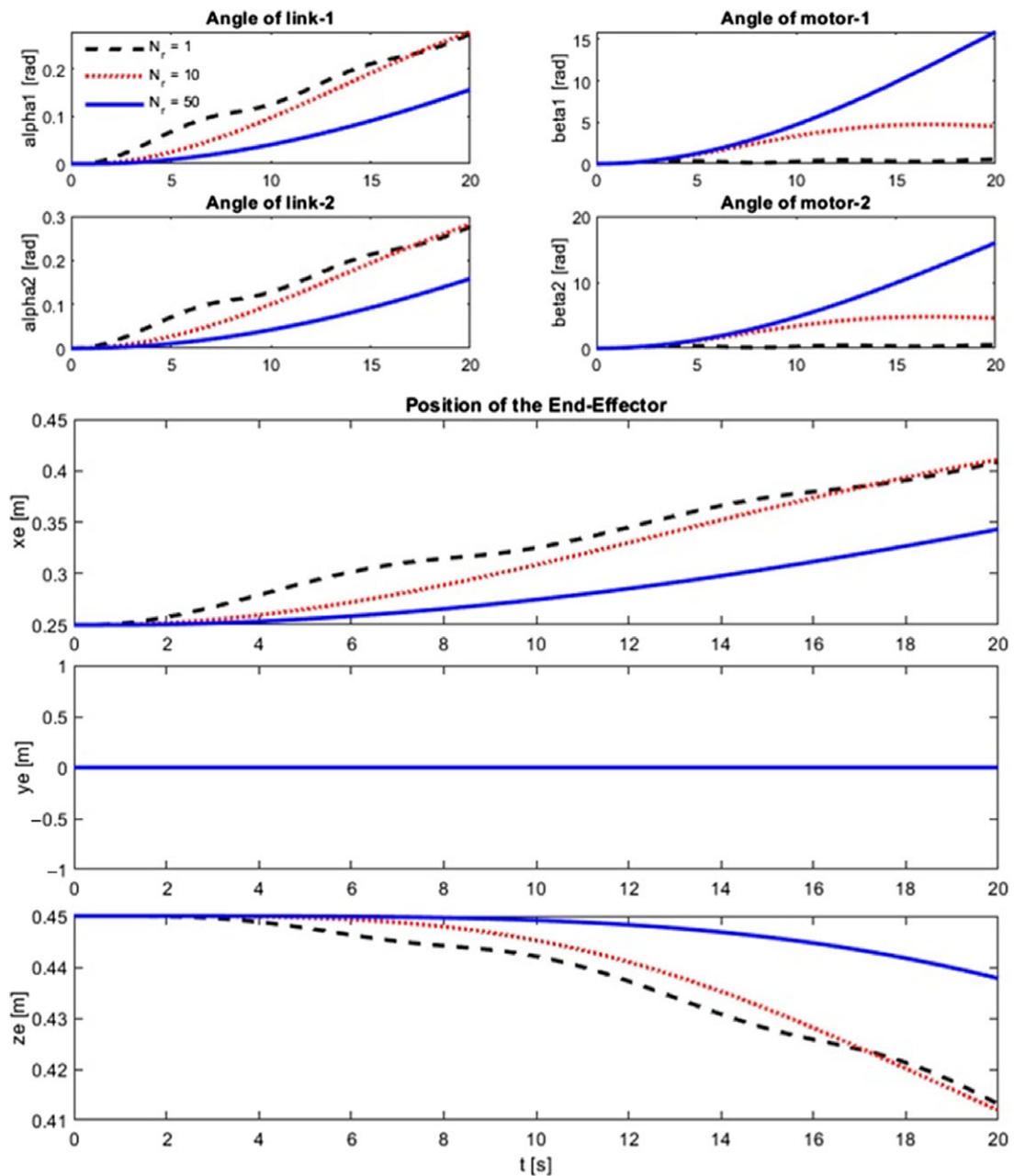


Fig. 4b. Manipulator dynamics with a fixed base – A comparison of rigid-joint configuration with flexible joints modeled as torsional springs with  $k_t = 0.6$ .

and 0.2 N-s/m). The values of the parameters defining the hysteretic torque are as follows:  $a = 161$ ,  $b = 0.1$ ,  $\sigma = 0.5$ ,  $n = 2.1$ . It can be seen that the responses of the end effector considering the flexible joint configuration are different from the responses resulting from the rigid-joint configuration. The plots for the positions of the end effector along the  $i$ -axis (i.e.,  $x_e$ ) and  $k$ -axis (i.e.,  $z_e$ ) indicate that joint flexibility imparts more oscillations to the responses as compared to the responses caused by the rigid-joint configuration. However, an increase in the damping of the joint attenuates the amplitude of the response of the end effector. The reduction in the areas of hysteresis loops (the two plots shown at the bottom) with the increase in the damping indicate a loss of energy that causes low amplitude oscillations.

Figure 5(b) illustrates the effect of the joint friction ( $f_j$ ), which is transmitted from the shaft of the actuator to the link, on the response of the end effector: The dashed line corresponds to the response due to the rigid joint, the dash-dot line indicates the response due to the flexible joint, modeled as a

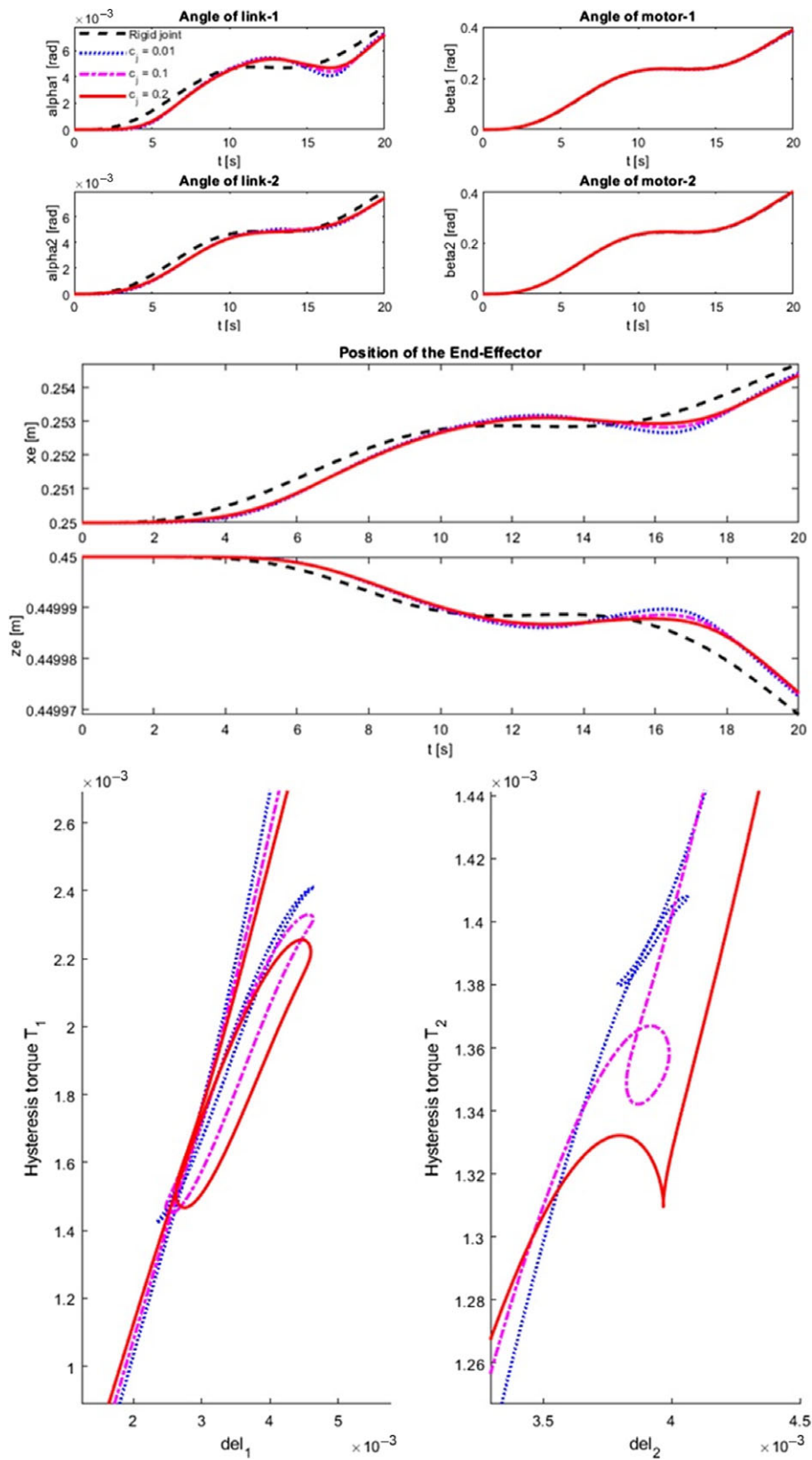


Fig. 5a. Manipulator dynamics with a fixed base – A comparison of rigid-joint configuration with flexible joints modeled as hysteretic springs, considering variation in joint damping ( $c_j$ ).

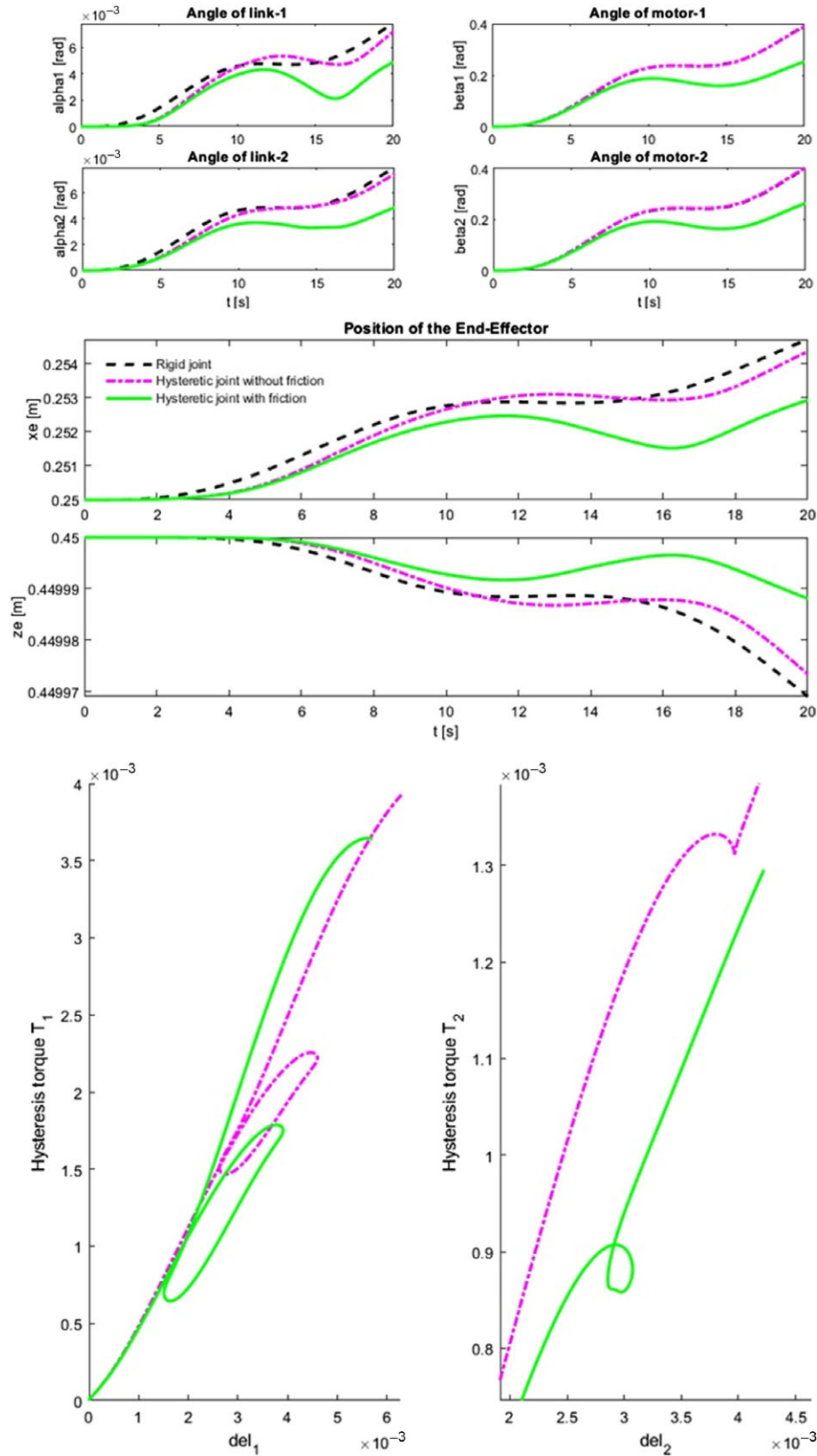


Fig. 5b. Manipulator dynamics with a fixed base – a comparison of rigid-joint configuration with flexible joints modeled as hysteretic springs with viscous damping and contact friction.

hysteretic spring without considering joint friction, whereas the solid line represents the response due to the hysteretic joint with friction. It is to be noted that in Fig. 5(b), the responses are obtained using a joint-damping value of  $c_j = 0.2$  N-s/m. It is evident from the plots of the positions of the end effector that when friction of the joints is included, it significantly reduces the amplitudes of oscillations and results in a large deviation of the responses from those corresponding to the rigid joint. The values of the parameters of the friction are given in Table I. Figure 6 compares the responses of the end effector considering all the three joint configurations discussed above, given that  $\tau_{\beta 1} = \tau_{\beta 2} = 0.01 \sin(0.5t)$  N-m. The response due to the rigid joint is represented by dashed line, due to the torsion spring configuration is represented by the dash-dot line, and due to the hysteretic spring configuration is represented by the solid line. It is clearly evident that the responses corresponding to the flexible-joint (modeled considering hysteresis and dynamic friction) are significantly different from the other two joint configurations. Therefore, the importance of considering the hysteresis and dynamic friction in modeling a flexible joint is clearly evident.

So far, the dynamics of the flexible joint manipulator was discussed when the vehicle was assumed to be at rest. Now, the effect of the movements of the vehicle on the responses of the manipulator will be included. First, the case of the movements of the vehicle caused by its interaction with sea currents is discussed. It is to be noted that, in this study, steady sea currents, having a constant velocity, are assumed in the simulations. Figure 7 compares the responses of the UVMS in the presence and absence of the sea currents when a rigid joint between the vehicle and the manipulator is used. The dash-dot lines in Fig. 7(a) show the responses of the UVMS upon its interaction with a current  $U = 0.03$  m/s along the  $i$ -axis whereas the solid lines depict the responses to a current  $U = 0.05$  m/s along the  $i$ -axis. When there are no currents, both the vehicle and the manipulator remain stationary, see the dashed lines. It is evident that the currents move the vehicle only along the  $i$ -axis. Since there is no actuation of the joints of the manipulator, the position of the end effector changes along the  $i$ -axis only. Since the current is along the  $i$ -axis, it interacts (head on) with the face of the vehicle and passes parallel to the surge axis of the vehicle. In such a configuration (i.e., when a cylindrical body is parallel to the flow of a fluid), the effect of the vortex-induced forces is minimal and thus is ignored in this set of simulations. However, when the currents act perpendicular to the surge axis of the vehicle (i.e., along the  $j$  and  $k$  axes), the fluid–structure interaction results in shedding of vortices from the surface of the vehicle in the direction perpendicular to that of the current. Consequently, a current along the  $j$ -axis induces VIVs in the vehicle along the  $k$ -axis whereas a current along the  $k$ -axis induces VIVs along the  $j$ -axis. The said VIV phenomenon is depicted in Fig. 7(b) and (c). Figure 7(b) shows that a current  $V = 0.03$  m/s acting on the vehicle along the  $j$ -axis moves the vehicle along both the  $j$  and  $k$  axes, see the dash-dot lines, where the movement along the  $j$ -axis is due to the drag force along the same direction and the oscillatory movement along the  $k$ -axis is due to the VIVs. When a current of higher magnitude (i.e.,  $V = 0.05$  m/s) interacts with the UVMS, it can be seen that the vibrations of the VIVs of the vehicle are increased (see the solid lines). Such VIVs are also transmitted to the manipulator as significant oscillations can be observed in the response of the end effector along the  $k$ -axis, see the dash-dot and solid lines. The responses of the vehicle and the end effector when  $V = 0$  m/s are represented in dashed lines. Similarly, Fig. 7(c) shows the transmission of VIVs from the vehicle to the end effector along the  $j$ -axis given by the dash-dot and the solid lines for end-effector's response along the  $j$ -axis when the UVMS encounters the currents  $W = 0.03$  m/s and  $W = 0.05$  m/s, respectively, along the  $k$ -axis.

After considering the effects of sea currents on the responses of the UVMS, now the effect of the translations and rotations of the vehicle on the dynamics of the manipulator will be discussed without considering the effects of the currents and movements of the links of the manipulator. Figure 8(a) shows that a force  $f_u = 1.0$  N translates the vehicle along the  $i$ -axis and, consequently, the position ( $x_e$ ) of the end effector along the  $i$ -axis. Figure 8(b) shows that force  $f_v = 1.0$  N translates the vehicle along the  $j$ -axis, which results in the shedding of vortices from the structure of the vehicle and, consequently, the vehicle exhibits VIVs along the  $k$ -axis. The said translational and vibratory motion of the vehicle along the  $j$  and  $k$  axes, respectively, is also evident in the response of the end effector. It can be seen that the end effector is translated along the  $j$ -axis while exhibiting VIVs along the  $k$ -axis. Similarly, Fig. 8(c) depicts that when a force  $f_w = 1.0$  N moves the vehicle along the  $k$ -axis, the vehicle also experiences VIVs along the  $j$ -axis. The transmittance of the VIVs to the manipulator is also evident in the position response  $y_e$  of the end effector along the  $j$ -axis.



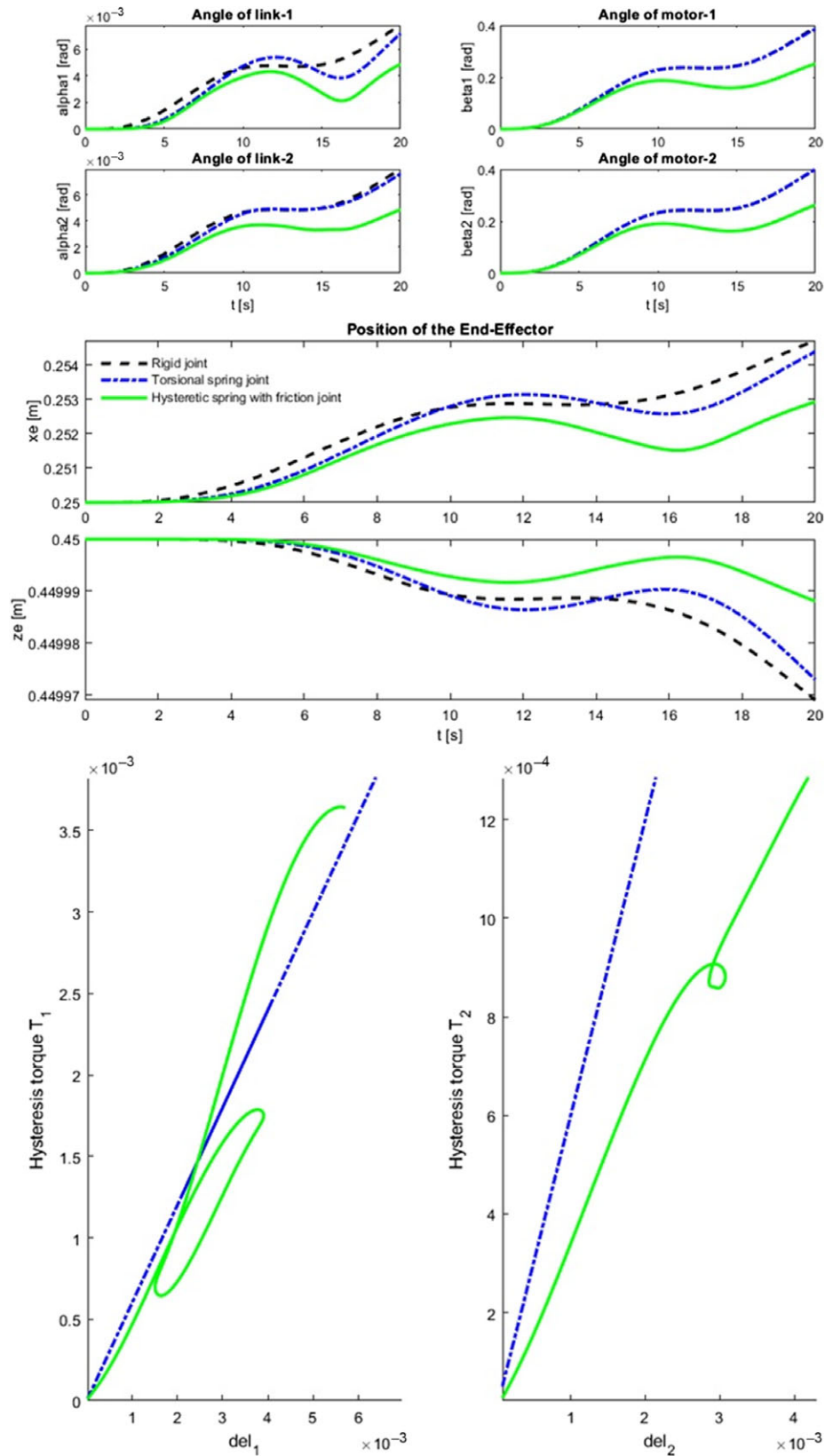


Fig. 6. Manipulator dynamics with a fixed base – A comparison of rigid-joint configuration with flexible joints modeled as torsional springs and hysteretic springs.

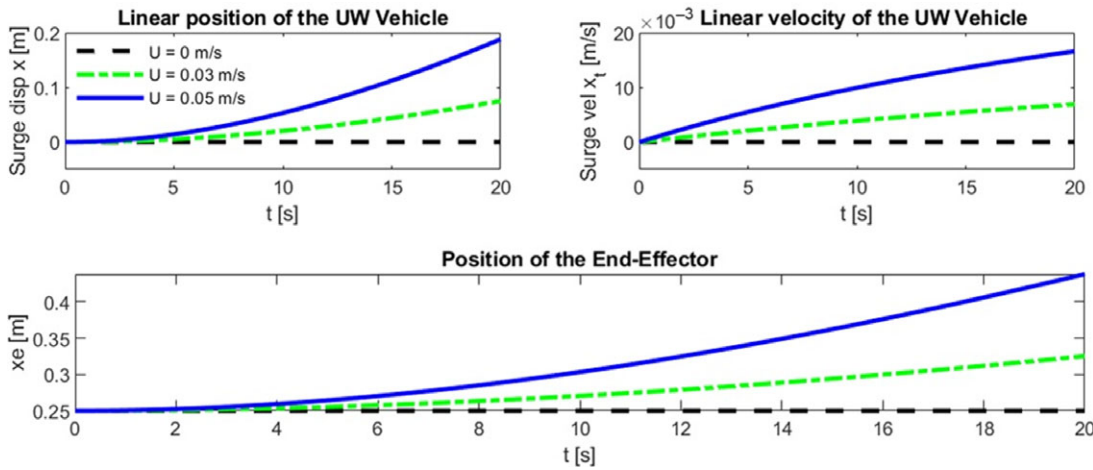


Fig. 7a. Effect of sea current (along the surge direction) on the dynamics of UVMS considering rigid joint between the AUV and the manipulator.

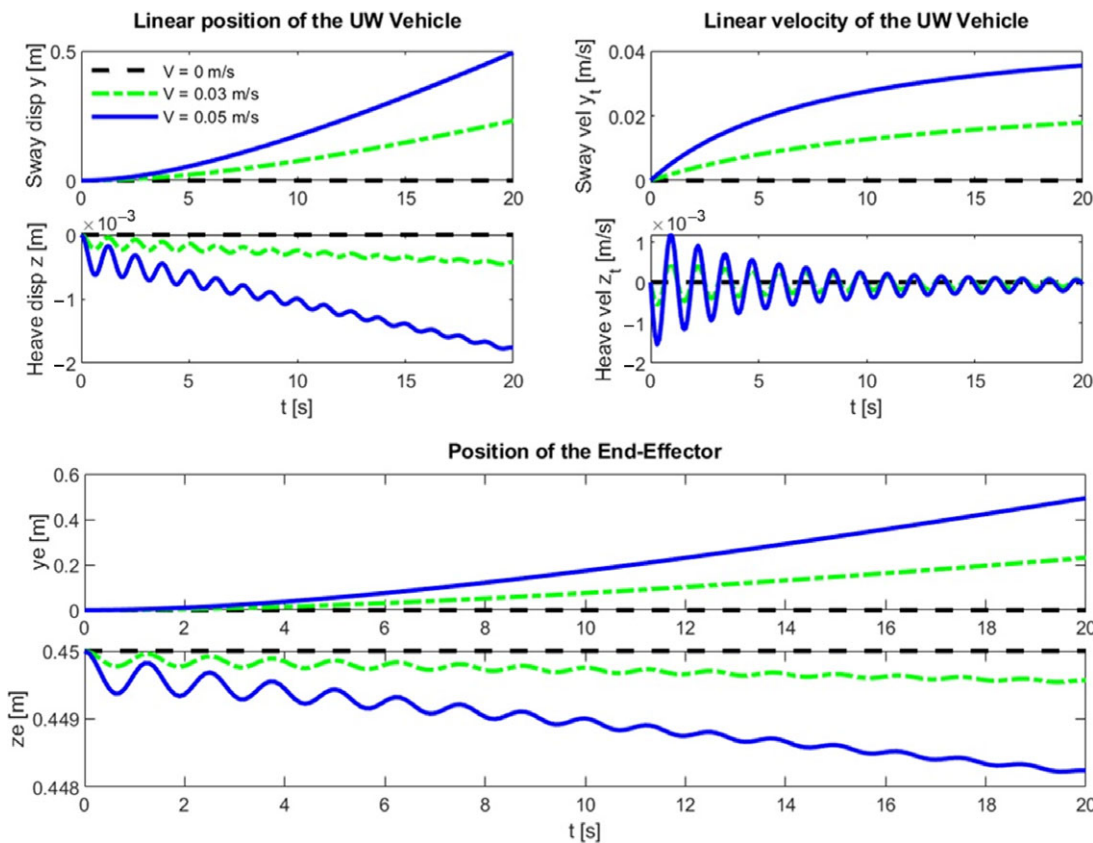


Fig. 7b. Effect of sea current (along the sway direction) on the dynamics of UVMS considering rigid joint between the AUV and the manipulator.

So far, only the responses of the manipulator upon translations of the vehicle are considered. Now, the effect of the rotations of the vehicle on the dynamics of the manipulator will be investigated. Figure 8(d) depicts that a torque  $\tau_p = 1.0$  N-m rotates the vehicle about the *i*-axis and, consequently, the position of the end effector changes along the *j* and *k* axes. Figure 8(e) shows that a torque  $\tau_q = 1.0$  N-m rotates the vehicle about the *j*-axis resulting in a change of the position of the manipulator along the *i* and *k* axes. Figure 8(f) shows that a torque  $\tau_r = 1.0$  N-m rotates the vehicle about the *k*-axis resulting in a change of the position of the manipulator along the *i*-axis only. The change in the

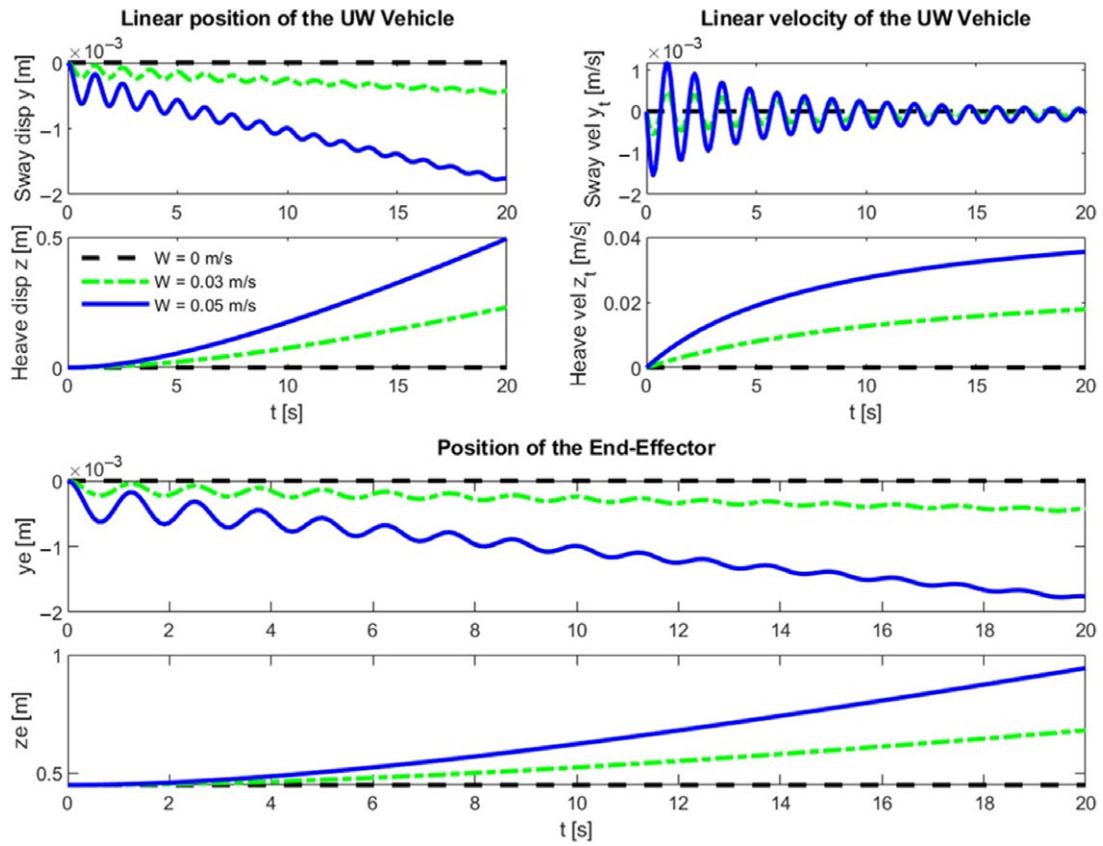


Fig. 7c. Effect of sea current (along the heave direction) on the dynamics of UVMS considering rigid joint between the AUV and the manipulator.

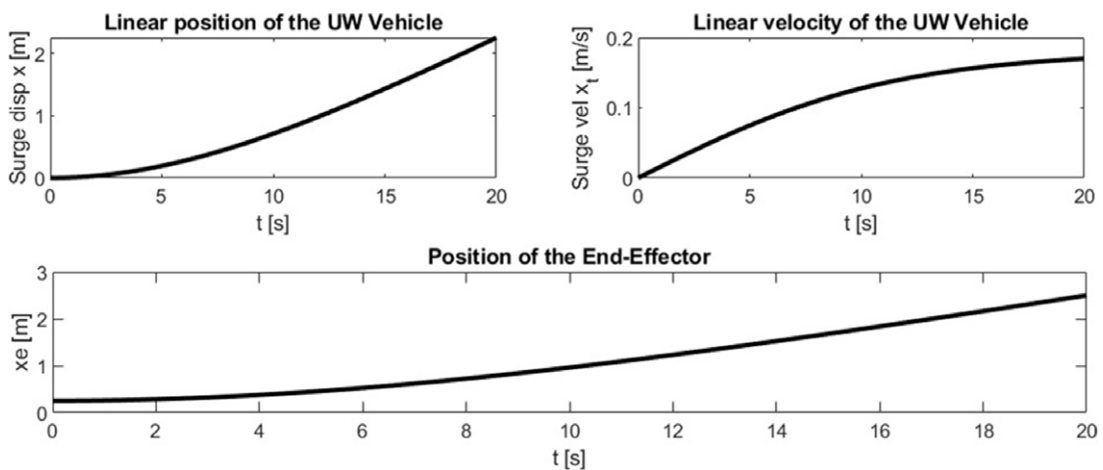


Fig. 8a. Effect of AUV translation, in surge direction, on the position of the end effector.

position of the end effector only along the *i*-axis indicates an offset, along the surge axis, of the base of the manipulator from the CG of the vehicle by 0.25 m.

The simulations generated so far investigate the effects of the movements of the vehicle on the dynamics of the manipulator only. However, Fig. 9 shows that the movements of the manipulator do not have any influence on the dynamics of the vehicle, that is, the pitch dynamics of the AUV are not changed. This is because the coupling between the manipulator and the vehicle is neglected in the previous set of simulations. Such a behavior is acceptable only if the mass of the manipulator

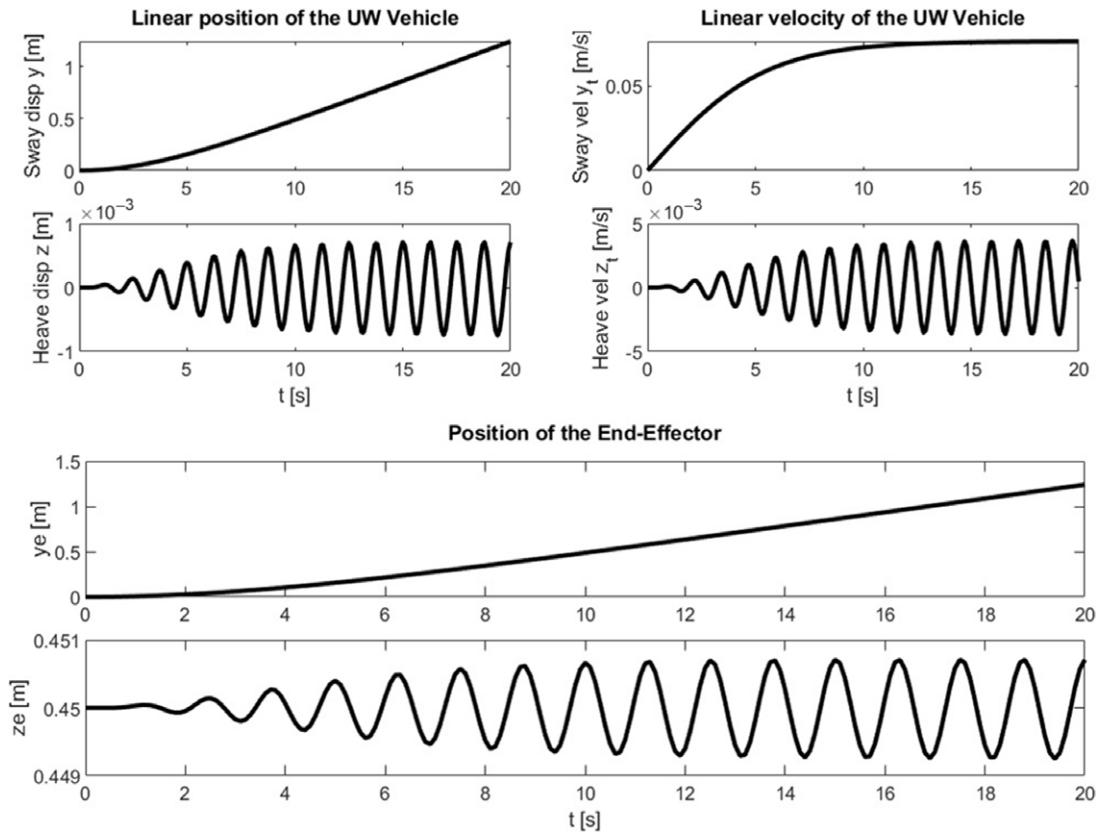


Fig. 8b. Effect of AUV translation, in the sway direction, on the position of the end effector.

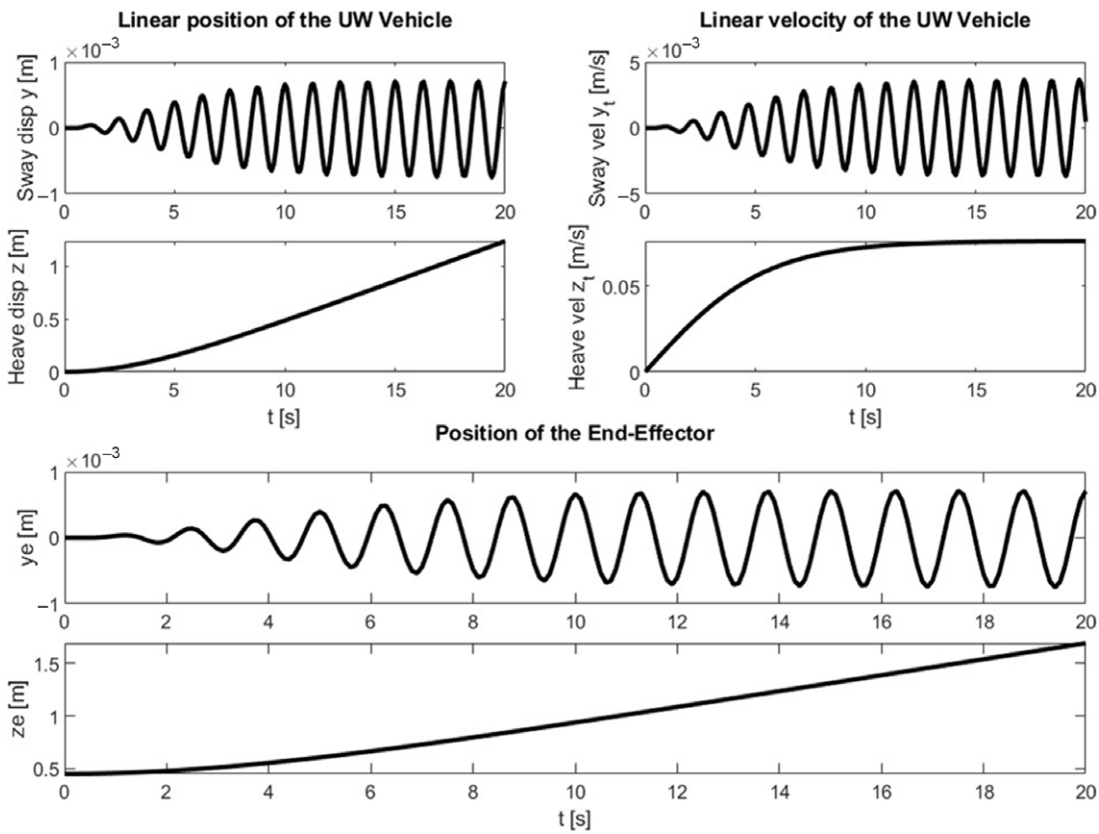


Fig. 8c. Effect of AUV translation, in the heave direction, on the position of the end effector.

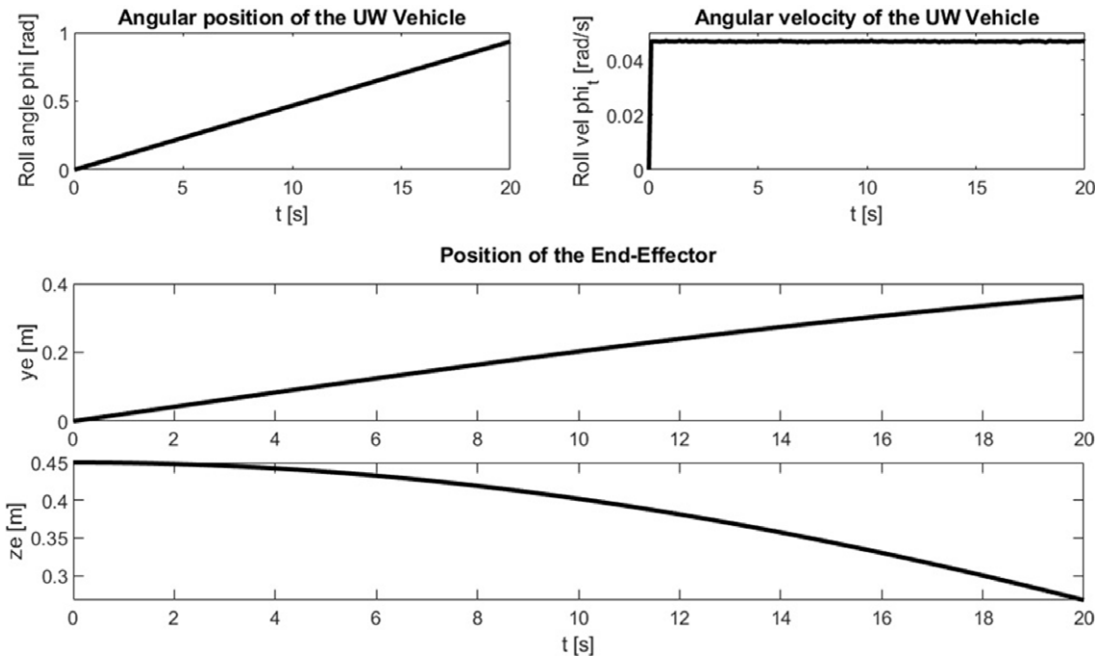


Fig. 8d. Effect of AUV rotation (roll) on the position of the end effector (considering no coupling between the AUV and the manipulator).

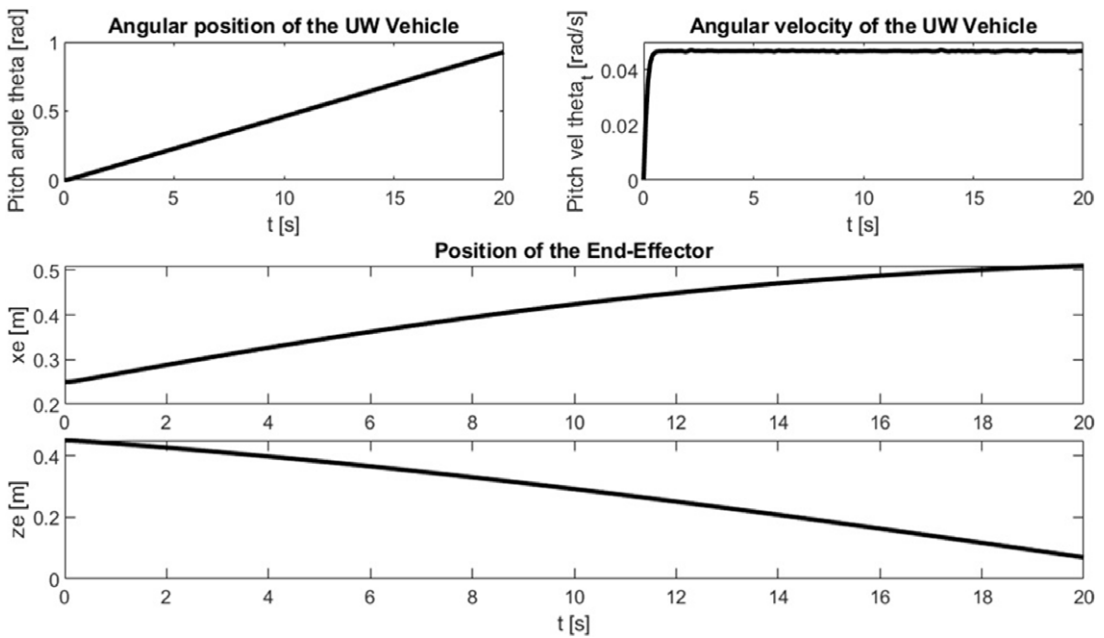


Fig. 8e. Effect of AUV rotation (pitch) on the position of the end effector (considering no coupling between the AUV and the manipulator).

is significantly less than that of the vehicle. However, in this work, it is assumed that the movement of the manipulator is coupled with the pitch dynamics of the vehicle and must be reflected in the dynamics of the UVMS by including the terms  $k_m(\alpha_1(t) - \theta(t))$  and  $k_m(\theta(t) - \alpha_1(t))$  on the right-hand side of the equations of the pitch motion of the vehicle and the first link of the manipulator. Figure 10 shows the effect of the movements of the manipulator on the dynamics of the vehicle,

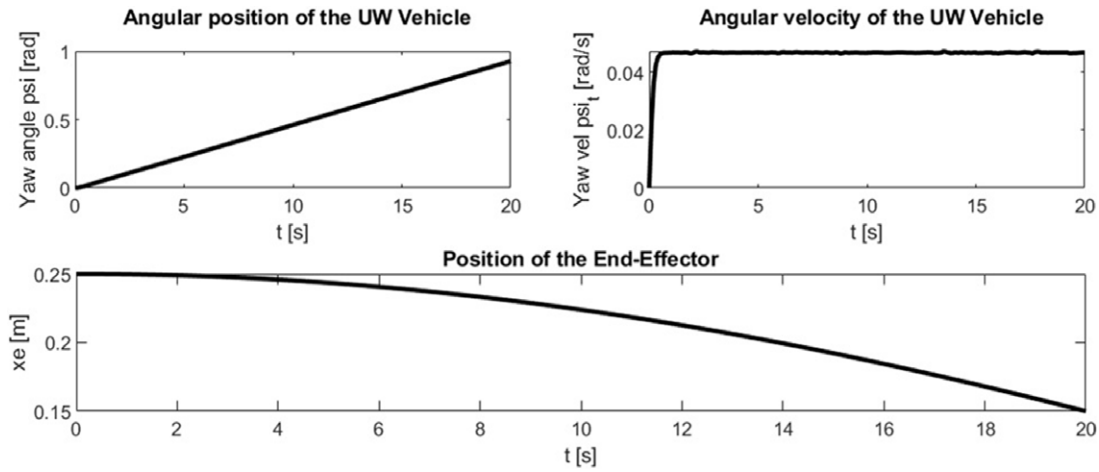


Fig. 8f. Effect of AUV rotation (yaw) on the position of the end effector (considering no coupling between the AUV and the manipulator).

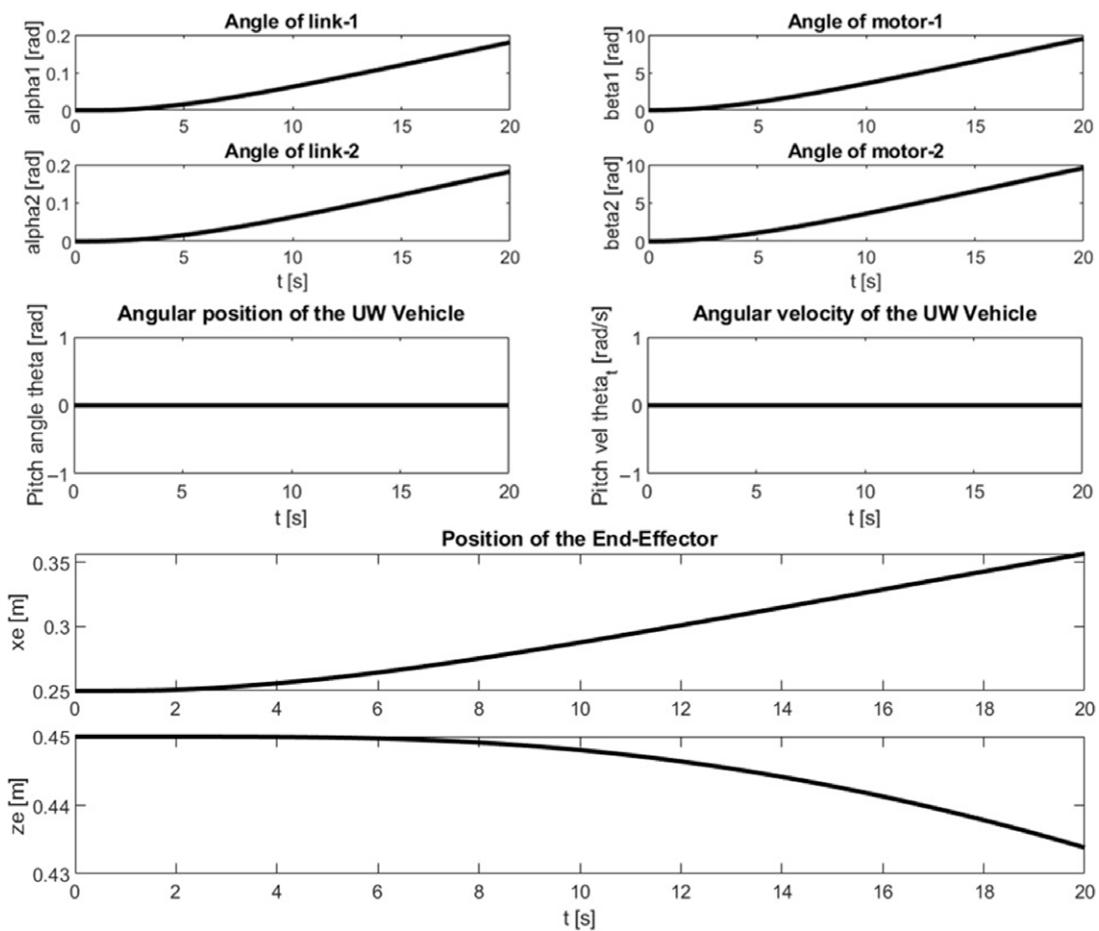


Fig. 9. Manipulator movements do not effect AUV dynamics when there is no coupling between the AUV and the manipulator.

after inclusion of the coupling between the manipulator and the vehicle. Variation in the coefficient of coupling  $k_m$  results in the transmittance of motion from the manipulator to the vehicle. In Fig. 10, the solid line represents the responses when coupling is not included whereas the dash-dot line, the dashed line, and the dotted line indicate responses for  $k_m = 0.005, 0.01,$  and  $0.02,$  respectively. It is

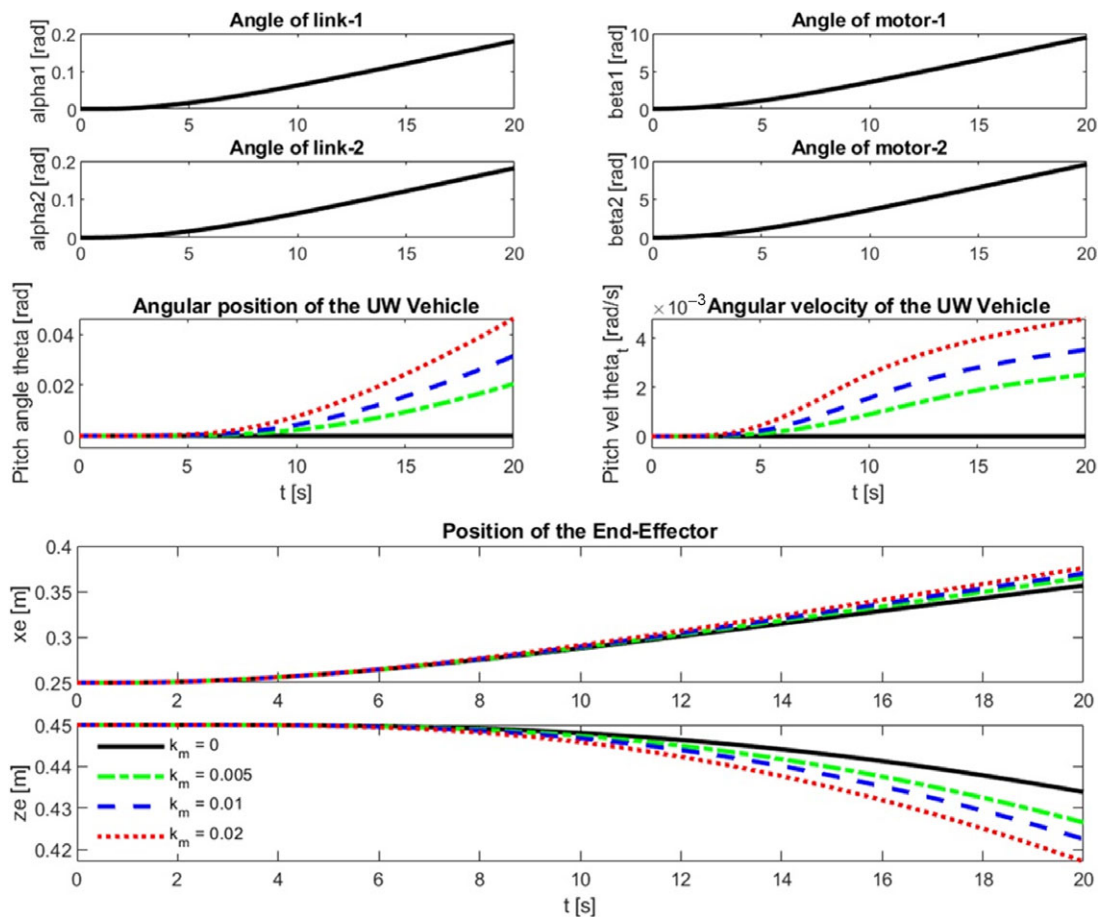


Fig. 10. Effect of manipulator movements on AUV dynamics.

evident that increasing the value of  $k_m$  accentuates the transmission of motion from the manipulator to the vehicle, which also results in deviation of the position of the end effector from that of the uncoupled response. By considering the coupling between the manipulator and the vehicle, the effect of the pitch movements of the vehicle on the response of the manipulator is also changed. Figure 11 presents the comparison of the responses of the end effector due to the pitch movements of the vehicle when coupling between the manipulator and the vehicle is not included (represented by the dashed line) and when  $k_m = 0.1$  (represented by the solid line). Finally, Fig. 12 shows the responses of the end effector considering all the movements of the vehicle and the manipulator for the cases when coupling between the manipulator and the vehicle is not considered (dashed line) and when  $k_m = 0.1$  (solid line).

In order to demonstrate the effect of the hydrodynamic forces on the UVMS, Fig. 13 provides a comparison of the responses of the end effector for the UVMS operation with and without consideration of the hydrodynamic forces. Figure 13(a) depicts the comparison of responses for the pitch movement of the vehicle. It can be seen that in the absence of the hydrodynamic forces, which in this case it is assumed as a friction/damping, the magnitudes of movements of both the vehicle and the end effector (shown in dashed lines) are larger when hydrodynamic forces are considered (shown as solid lines in Fig. 13(a)). The pitch movement of the vehicle in water involves only the drag, viscous damping, and added mass forces. Finally, the VIV effect is also included in the simulations and the results are shown in Fig. 13(b) which depicts the end-effector's responses when the vehicle exhibits heave motion. It can be seen that in the absence of hydrodynamic forces, the end effector moves only along the  $k$ -axis, see the dashed line. However, in the presence of the hydrodynamic forces, VIVs

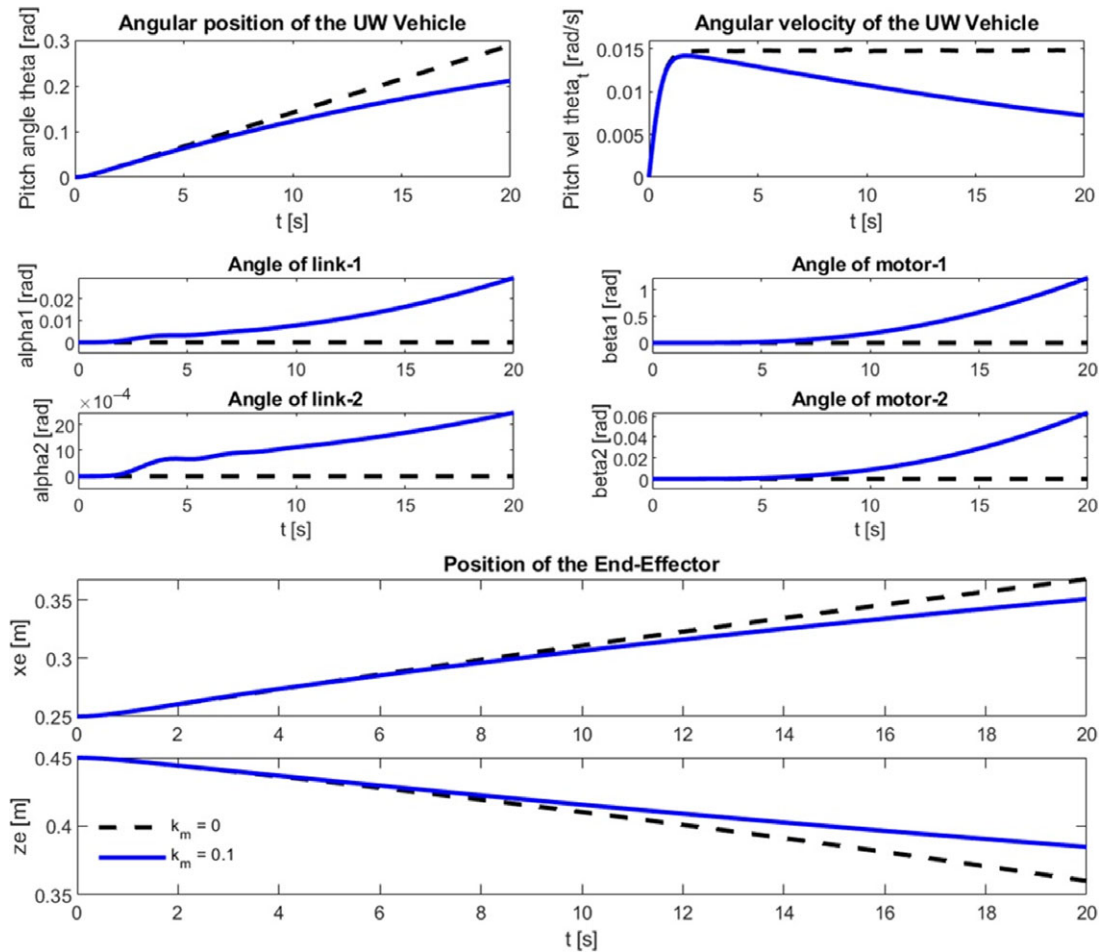


Fig. 11. Effect of AUV rotation (pitch) on the EE position considering coupling between AUV and the manipulator.

are induced along the  $j$ -axis of the vehicle. Moreover, due to the coupling between the vehicle and the manipulator, the said vibrations are also transmitted to the end effector, see the solid line for the response of the end effector along the  $j$ -axis. Finally, Fig. 13(c) compares the response of the end effector for simultaneous pitch and heave motions of the vehicle in the air, represented by dashed lines, and in water, represented by solid lines. Hence, from Fig. 13, the effect of the hydrodynamic forces on the response of both the vehicle and the end effector is clearly visible.

#### 4. Results and Conclusion

A detailed mathematical model of the UVMS, consisting of an underwater autonomous vehicle affixed with a flexible-joint two-link manipulator, is derived using the quasi-Lagrange formulation. In order to model the fluid–structure interaction, the added mass forces, buoyancy forces, viscous damping forces, and the nonlinear drag and vortex-induced forces are accounted for. Further, flexible-joint configuration of the manipulator was considered, where the interface of the joints’ motor with the links was modeled as a hysteretic spring having additional dynamic as well as viscous friction. The study presented here revealed that the flexibility of the joints of the manipulator and the VIVs transmitted from the AUV to the manipulator significantly affect the positions of the end effector and must be incorporated in developing a control model for the UVMS to perform precise manipulation tasks in water.



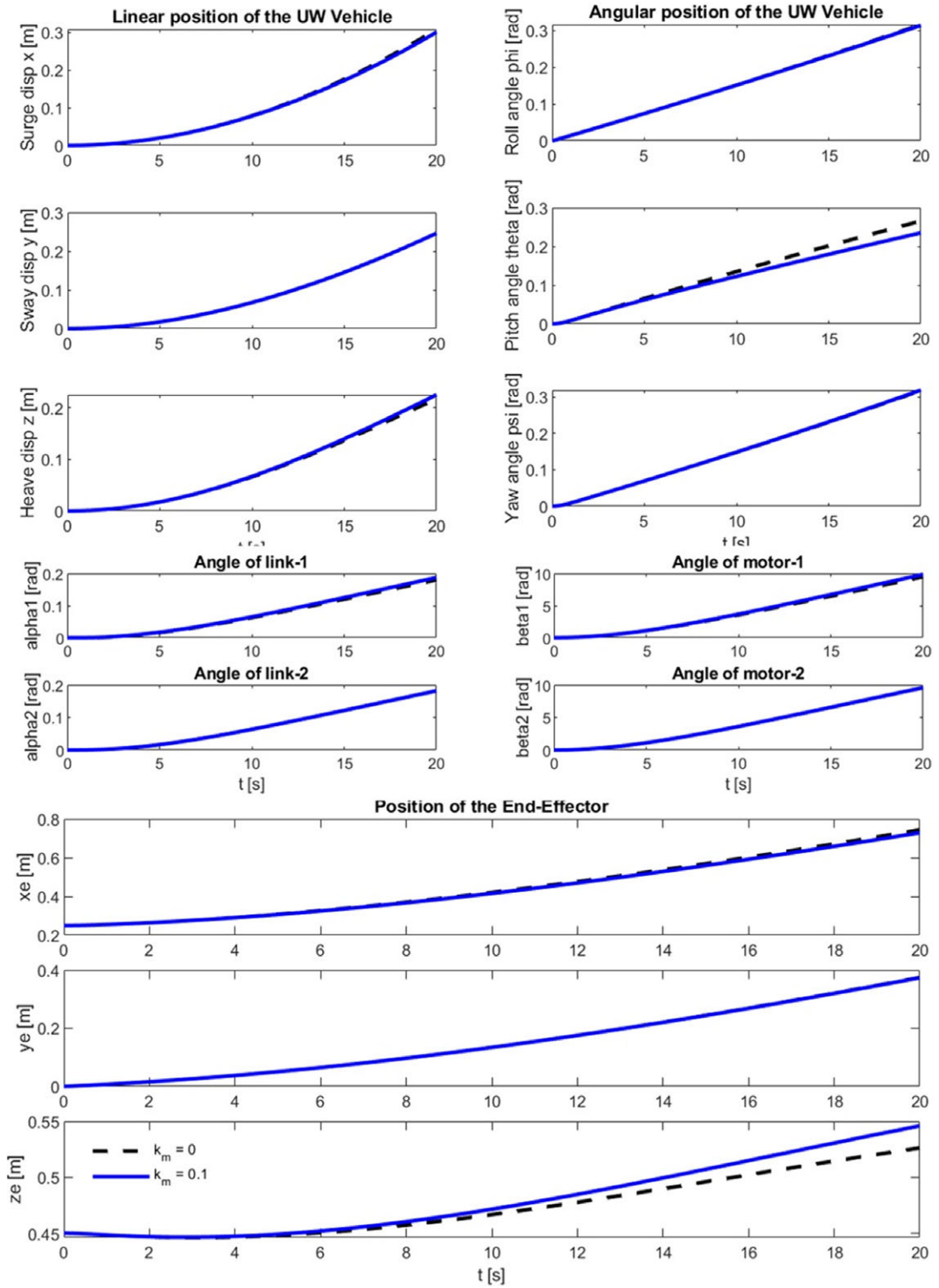


Fig. 12. Complete UVMS operation considering rigid and flexible joints.

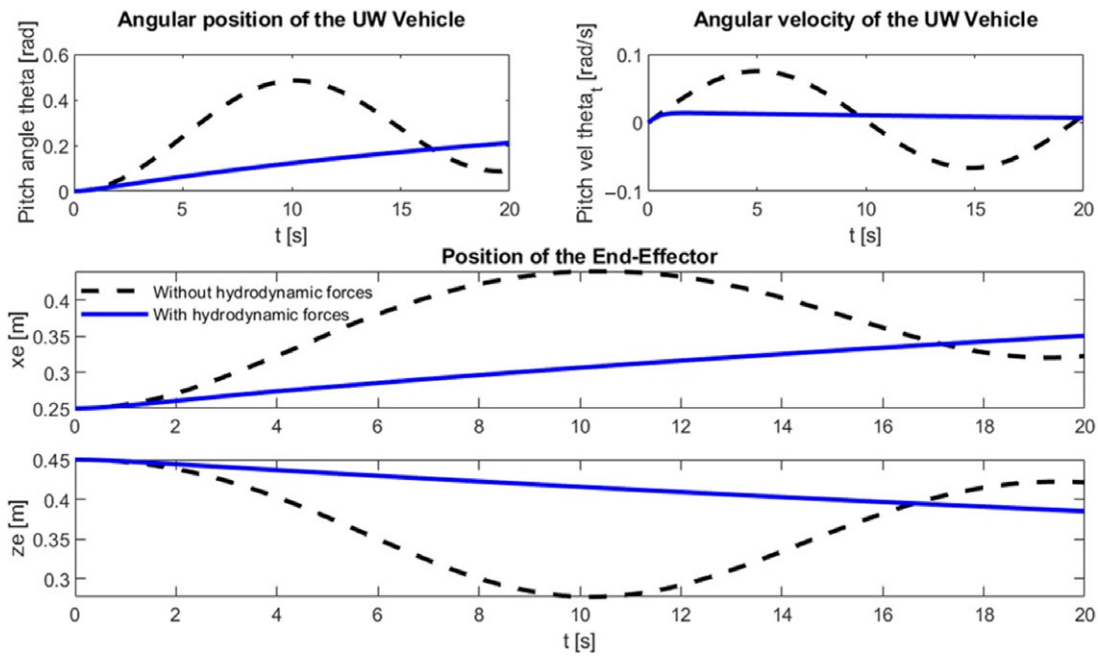


Fig. 13a. Responses of the end effector while considering and neglecting the hydrodynamic forces upon pitch motion of the vehicle.

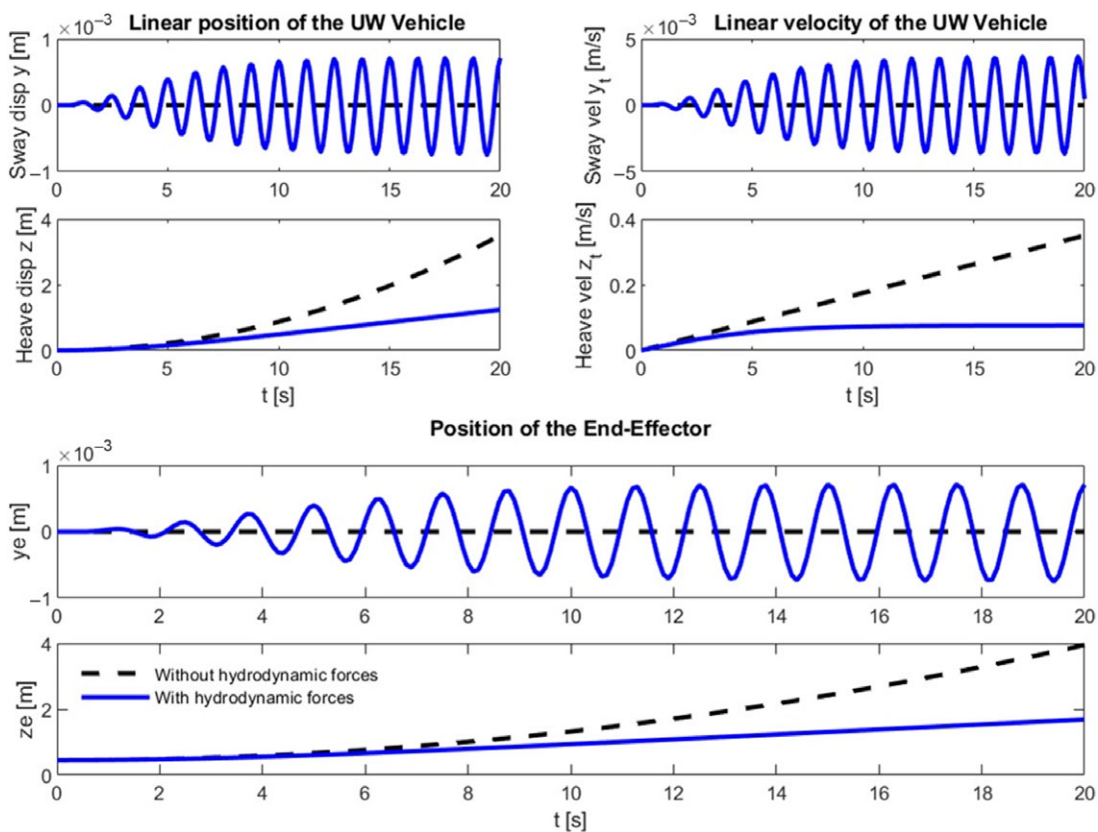


Fig. 13b. Responses of the end effector while considering and neglecting the hydrodynamic forces upon heave motion of the vehicle.

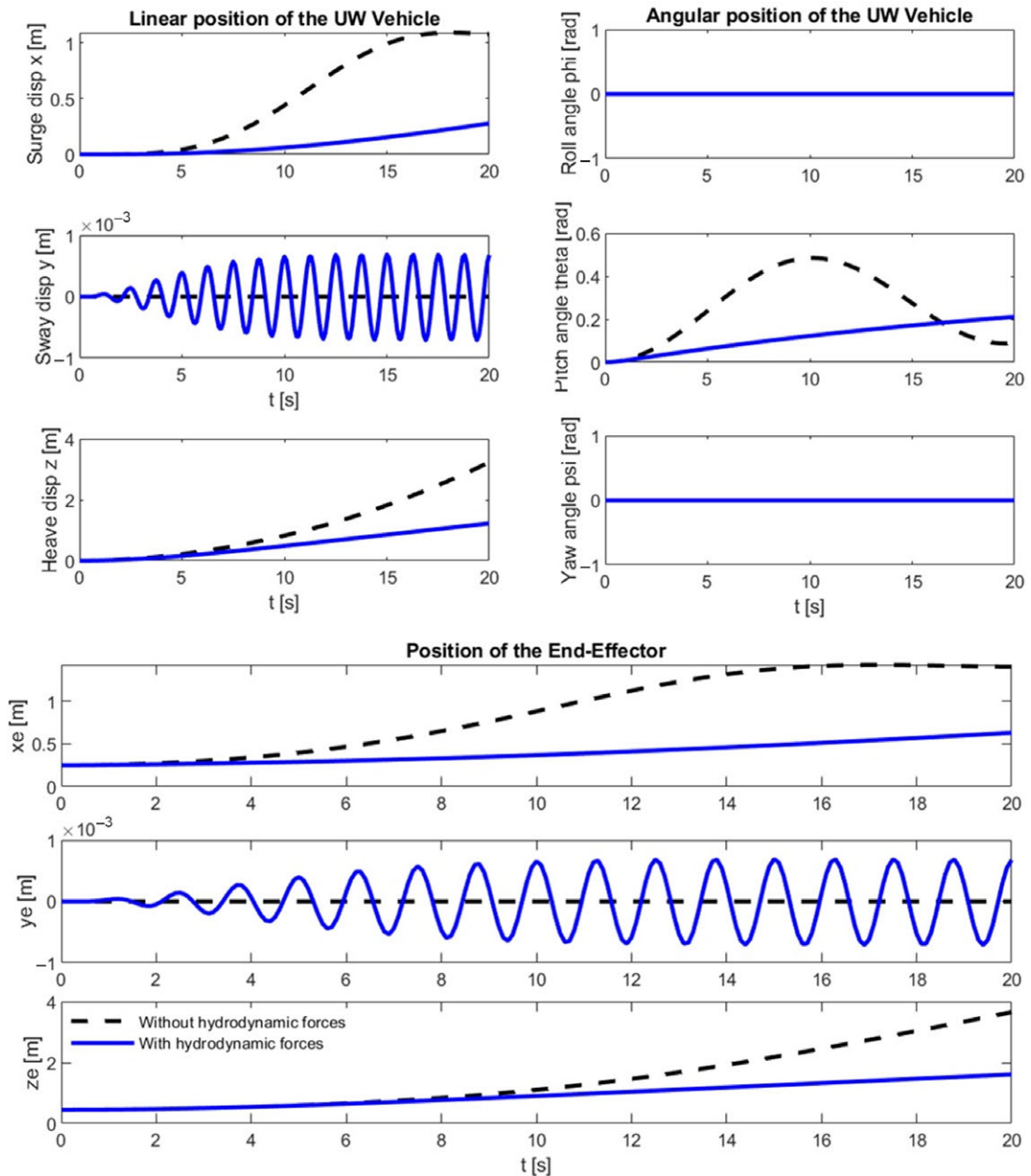


Fig. 13c. Responses of the end effector while considering and neglecting the hydrodynamic forces upon pitch and heave motions of the vehicle.

### Conflict of Interest

Drs. U.H. Shah, M. Karkoub, D. Kerimoglu, and H.-D. Wang have no conflicts of interest or financial ties to disclose.

### Supplementary Material

To view supplementary material for this article, please visit <https://doi.org/10.1017/S0263574721000072>.

## References

1. T. W. Kim, G. Marani and J. Yuh, "Underwater vehicle manipulators," **In: Springer Handbook of Ocean Engineering. Springer Handbooks** (M. R. Dhanak and N. I. Xiros, eds) (Springer, Cham, 2016). doi: [10.1007/978-3-319-16649-0\\_17](https://doi.org/10.1007/978-3-319-16649-0_17).
2. B. O. A. Haugalokken, E. K. Jorgensen and I. Schjolberg, "Experimental validation of end-effector stabilization for underwater vehicle-manipulator systems in subsea operations," *Robot. Autom. Syst.* **109**, 1–12 (2018). doi: [10.1016/j.robot.2018.08.007](https://doi.org/10.1016/j.robot.2018.08.007).
3. H. Shim, B. H. Jun, P. M. Lee, H. Baek and J. Lee, "Workspace control system of underwater tele-operated manipulators on an ROV," *Ocean Eng.* **37**(11–12), 1036–1047 (2010). doi: [10.1016/j.oceaneng.2010.03.017](https://doi.org/10.1016/j.oceaneng.2010.03.017).
4. Y. Wang, S. Wang, Q. Wei, M. Tan, C. Zhou and J. Yu, "Development of an underwater manipulator and its free-floating autonomous operation," *IEEE-ASME Trans. Mechatron.* **21**(2), 815–824 (2016). <https://ieeexplore.ieee.org/document/7303960>.
5. M. Karkoub, H. M. Wu and C. L. Hwang, "Nonlinear trajectory-tracking control of an autonomous underwater vehicle," *Ocean Eng.* **145**, 188–198 (2017). doi: [10.1016/j.oceaneng.2017.08.025](https://doi.org/10.1016/j.oceaneng.2017.08.025).
6. T. I. Fossen, *Guidance and Control of Ocean Vehicles* (John Wiley & Sons, New York, NY, USA, 1994). ISBN: 978-0471941132.
7. I. Schjolberg and T. I. Fossen, "Modelling and Control of Underwater Vehicle-Manipulator System," *Proceedings of Marine Craft Maneuvering and Control* (1994) pp. 45–57.
8. M. W. Dunnigan and G. T. Russell, "Evaluation and reduction of the dynamic coupling between a manipulator and an underwater vehicle," *IEEE J. Ocean. Eng.* **23**(3), 260–273 (1998). <https://ieeexplore.ieee.org/document/701201>.
9. M. Santhakumar, "Investigation into the dynamics and control of an underwater vehicle-manipulator system," *Modelling Simul. Eng.*, 1–13 (2013). doi: [10.1155/2013/839046](https://doi.org/10.1155/2013/839046).
10. C. Barbalata, M. W. Dunnigan and Y. Petillot, "Coupled and decoupled force/motion controllers for an underwater vehicle-manipulator system," *J. Mar. Sci. Eng.* **6**, (2018). doi: [10.3390/jmse6030096](https://doi.org/10.3390/jmse6030096).
11. N. Sarkar and T. K. Podder, "Coordinated motion planning and control of autonomous underwater vehicle-manipulator systems subject to drag optimization," *IEEE J. Ocean. Eng.* **26**(2), 228–239 (2001). <https://ieeexplore.ieee.org/document/922789>.
12. T. J. Tarn, G. A. Shoults and S. P. Yang, "A dynamic model of an underwater vehicle with a robotic manipulator using Kane's method," *Auton. Robot.* **3**(2–3), 269–283 (1996). doi: [10.1007/BF00141159](https://doi.org/10.1007/BF00141159).
13. B. Levesque and M. J. Richard, "Dynamic analysis of a manipulator in a fluid environment," *Int. J. Robot. Res.* **13**(3), 221–231 (1994). doi: [10.1177/027836499401300304](https://doi.org/10.1177/027836499401300304).
14. S. McMillan, D. E. Orin and R. B. McGhee, "Efficient dynamic simulation of an underwater vehicle with a robotic manipulator," *IEEE Trans. Syst. Man Cybern.* **25**(8), 1194–1206 (1995). doi: [10.1109/21.398681](https://doi.org/10.1109/21.398681).
15. K. -S. Hong and U. H. Shah, "Vortex-induced vibrations and control of marine risers: A review," *Ocean Eng.* **152**, 300–315 (2018). doi: [10.1016/j.oceaneng.2018.01.086](https://doi.org/10.1016/j.oceaneng.2018.01.086).
16. U. H. Shah and K.-S. Hong, "Active vibration control of a flexible rod moving in water: Application to nuclear refueling machines," *Automatica* **93**, 231–243 (2018). doi: [10.1016/j.automatica.2018.03.048](https://doi.org/10.1016/j.automatica.2018.03.048).
17. C. H. K. Williamson and R. Govardhan, "Vortex-induced vibrations," *Annu. Rev. Fluid Mech.* **36**(1), 413–455 (2004). doi: [10.1146/annurev.fluid.36.050802.122128](https://doi.org/10.1146/annurev.fluid.36.050802.122128).
18. M. W. Spong, "Modeling and control of elastic joint robots," *J. Dyn. Syst. Meas. Control-Trans. ASME* **109**(4), 310–319 (1987). doi: [10.1115/1.3143860](https://doi.org/10.1115/1.3143860).
19. M. Ruderman, "Modeling of elastic robot joints with nonlinear damping and hysteresis," **In: Robotic Systems – Applications, Control and Programming, Intech Open** (2012). doi: [10.5772/25494](https://doi.org/10.5772/25494).
20. S. Ulrich, J. Z. Sasiadek and I. Barkana, "Modeling and direct adaptive control of a flexible-joint manipulator," *J. Guid. Control Dyn.* **35**(1), 25–39 (2012). doi: [10.2514/1.54083](https://doi.org/10.2514/1.54083).
21. S. R. Li, Z. L. Shao, P. D. Xu and H. Q. Yin, "Robust adaptive control for coordinated constrained multiple flexible joint manipulators with hysteresis loop," *Math. Probl. Eng.* (2018). doi: [10.1155/2018/2507637](https://doi.org/10.1155/2018/2507637).
22. A. Khalid and S. Mekid, "Intelligent spherical joints based tri-actuated spatial parallel manipulator for precision applications," *Robot. Comput.-Integr. Manuf.* **54**, 173–184 (2018). doi: [10.1016/j.rcim.2017.11.005](https://doi.org/10.1016/j.rcim.2017.11.005).
23. M. I. Awad, D. Gan, I. Hussain, A. Az-Zu'bi, C. Stefanini, K. Khalaf, Y. Zweiri, J. Dias and L. Seneviratne, "Design of a novel passive binary-controlled variable stiffness joint (BPVSJ) towards passive haptic interface application," *IEEE Access* **6**, 63045–63057 (2018). doi: [10.1109/ACCESS.2018.2876802](https://doi.org/10.1109/ACCESS.2018.2876802).
24. M. I. Awad, I. Hussain, D. Gan, A. Az-Zu'bi, C. Stefanini, K. Khalaf, Y. Zweiri, T. Taha, J. Dias and L. Seneviratne, "Passive discrete variable stiffness joint (PDVSJ-II): Modeling, design, characterization, and testing toward passive haptic interface," *J. Mech. Robot.* **11**(1), (2019), Article 011005. doi: [10.1115/1.4041640](https://doi.org/10.1115/1.4041640).
25. M. Ruderman, "Compensation of nonlinear torsion in flexible joint robots: Comparison of two approaches," *IEEE Trans. Ind. Electron.* **63**(9), 5744–5751 (2016). doi: [10.1109/TIE.2016.2574299](https://doi.org/10.1109/TIE.2016.2574299).
26. L. Meirovitch, *Methods of Analytical Dynamics* (Mc-Graw-Hill, New York, NY, USA, 1970). ISBN: 0-486-43239-4.
27. H. Baruh, *Analytical Dynamics* (McGraw-Hill, New York, NY, USA, 1999). ISBN: 0-07-365977-0.
28. M. Ruderman, T. Bertram and M. Iwasaki, "Modeling, observation, and control of hysteresis torsion in elastic robot joints," *Mechatronics* **24**(5), 407–415 (2014). doi: [10.1016/j.mechatronics.2014.02.009](https://doi.org/10.1016/j.mechatronics.2014.02.009).

29. C.-C. Lin, R.-C. Chen and T.-L. Li, "Experimental determination of the hydrodynamic coefficients of an underwater manipulator," *J. Robot. Syst.* **16**(6), 329–338 (1999). doi: [10.1002/\(SICI\)1097-4563\(199906\)16:6<329::AID-ROB2>3.0.CO;2-5](https://doi.org/10.1002/(SICI)1097-4563(199906)16:6<329::AID-ROB2>3.0.CO;2-5).
30. O. Marzouk, A. H. Nayfeh, I. Akhtar and H. N. Arafat, "Modeling steady-state and transient forces on a cylinder," *J. Vib. Control* **13**(7), 1065–1091 (2007). doi: [10.1177/1077546307078737](https://doi.org/10.1177/1077546307078737).
31. W. He, S. S. Ge, B. V. E. How, Y. S. Choo and K. -S. Hong, "Robust adaptive boundary control of a flexible marine riser with vessel dynamics," *Automatica* **47**(4), 722–732 (2011). doi: [10.1016/j.automatica.2011.01.064](https://doi.org/10.1016/j.automatica.2011.01.064).
32. U. H. Shah, M. Karkoub, H. D. Wang and D. Kerimoglu, "Effect of Manipulator's Joints Flexibility on the Positioning Precision of the End-Effector of the UVMS," *Dynamic Systems and Control Conference ASME*, vol. 59148, V001T03A008 (2019).
33. H. D. Wang, Z. Lin, M. Karkoub and D. Kerimoglu, "Extended State Observer Based Sliding Mode Control with Prescribed Performance for Underwater Vehicle Manipulator System," *5th International Conference on Automation, Control and Robotics Engineering (CACRE)* (IEEE, 2020) pp. 368–372.